

B 4 An introduction into optimal control for quantum technologies

Frank K. Wilhelm¹, Susanna Kirchhoff¹, Shai Machnes¹,
Nicolas Wittler¹, and Dominique Sugny²

¹Theoretical Physics, Saarland University, 66123
Saarbrücken

²Laboratoire Interdisciplinaire Carnot de Bourgogne (ICB)
UMR 6303 CNRS-Université Bourgogne-Franche Comté,
21078 Dijon Cedex, France

Contents

1	Introduction	3
2	Elementary optimal control	4
2.1	Optimal control of a classical harmonic oscillator	4
2.2	Optimal control for a classical system	5
2.3	Gradient-based optimal quantum control with the GRAPE algorithm	8
2.4	The Krotov algorithms	12
2.5	Modern numerical issues	12
3	Applied optimal quantum control	16
3.1	Closing the loop for pulse calibration	17
3.2	CRAB	18
3.3	GOAT	19
3.4	Evaluating fidelity with randomized benchmarking.	20
3.5	Approximating time evolutions with the Magnus expansion	24
3.6	Real-world limitations	26

4	Examples	27
4.1	Optimal control of a qubit	27
4.2	Exploring the speed limit with high parameter counts	27
4.3	Open systems	29
4.4	DRAG and its derivatives	30
5	Summary and outlook	35
	References	35

1 Introduction

Control is a key component in turning science into technology [20], [1]. Broadly and colloquially speaking, control looks at providing the user / experimenter with external parameters to steer a given dynamical system to her liking ¹ rather than simply observing its internal dynamics. Control is in this sense ubiquitous to modern technology. In this colloquial sense, quantum control is transferring that idea to quantum systems and thus contains both hard- and software of many kinds.

The ubiquity of control has given rise to the field of control theory. This is a field of applied mathematics that looks at how to choose said external parameters in order to drive the dynamical system to one's liking. It has spawned ideas of open-loop control, i.e., the pre-determination of controls given the laws of nature (that were a key ingredient to, e.g., the Apollo program) as well as closed-loop-control, interleaving of observation and adjustment as we know it in our daily lives from thermostats. This type of optimal control theory takes the hardware setup as a given, however ideally, these are developed in tandem. The mathematical procedures of open-loop-control typically involve optimizing a cost function, hence the name optimal control.

The application of optimal control is not an entirely new idea. Pioneering applications were primarily chemistry, such as the laser control of chemical reactions and magnetic resonance. By now, quantum optimal control is also applied to a large spectrum of modern quantum technologies (Quantum 2.0) [1]. This implies a certain tradition of fragmentation - quantum optimal control researchers tend to be in departments of mathematics, chemistry, computer science, and physics and follow their specific idiosyncrasies [20]. Modern efforts have gone very far in overcoming this fragmentation which is fruitful in learning from each other and respecting the different goals – quantum control of complex reactions does for example deal with large Hilbert spaces whereas control in quantum computing aims at sufficiently low errors in order to meet error correction thresholds.

In this series of lectures, we would like to introduce the audience to quantum optimal control. The first lecture will cover basic ideas and principles of optimal control with the goal of demystifying its jargon. The second lecture will describe computational tools (for computations both on paper and in a computer) for its implementation as well as their conceptual background. The third chapter will go through a series of popular examples from different applications of quantum technology.

These are lectures notes. Other than a textbook, it makes a significant difference to attend the lectures it goes with rather than use it to self-study. Other than a review, it is not complete but rather serves to introduce clarify the concepts of the field. This also means that the choice of references is certainly not complete, rather, it is the subjective choice of what the authors find most suitable and got inspired by.

¹ where female attributions are the default, male is considered included

2 Elementary optimal control

We start with classical examples of control, which lay a lot of foundations for quantum systems.

2.1 Optimal control of a classical harmonic oscillator

In order to understand the basic concept and structure of quantum optimal control, let us start with a simple classical example: control of the harmonic oscillator.

The equation of motion of a harmonic oscillator driven by force $F(t) = mf(t)$ where m is the mass and eigenfrequency Ω is given by

$$\ddot{x} + \Omega^2 x(t) = f(t).$$

Its general solution is parameterized through the Green's function

$$G(\tau) = \frac{\theta(\tau)}{\Omega} \sin(\Omega\tau)$$

(where θ is the Heaviside function) as

$$x(t) = x(0) \cos \Omega t + \frac{\dot{x}(0)}{\Omega} \sin \Omega t + \int_0^t dt' \frac{\sin \Omega(t-t')}{\Omega} f(t')$$

Readers not familiar with Green's functions can easily verify that this expression does indeed solve the equation of motion of the driven oscillator.

From this we get the velocity

$$\dot{x}(t) = \dot{x}(0) \cos \Omega t - \Omega x(0) \sin \Omega t + \int_0^t dt' \cos \Omega(t-t') f(t')$$

Thus, imposing target values $x(T)$ and $\dot{x}(T)$ we find the conditions

$$\begin{aligned} x(T) - x(0) \cos \Omega T - \frac{\dot{x}(0)}{\Omega} \sin \Omega T &= \int_0^T dt' \frac{\sin \Omega(T-t')}{\Omega} f(t') \\ \dot{x}(T) - \dot{x}(0) \cos \Omega T + \Omega x(0) \sin \Omega T &= \int_0^T dt' \cos \Omega(T-t') f(t'). \end{aligned}$$

These equations allow a few observations that have analogies all over quantum control: Firstly, the control $f(t)$ is needed to push the system away from its natural dynamics (the terms on the left) – it is redirecting the natural drift of the system. Secondly, there are two constraints for a function given through an integral – so we can expect many solutions. As an example, let's look at the case that we move a particle by a fixed distance $x(0) = 0$ and $x(T) = X$ from rest to rest $\dot{x}(T) = \dot{x}(0) = 0$. We thus need to satisfy

$$\int_0^T dt' \sin[\Omega(t-t')] f(t') = \Omega X \quad \int_0^T dt' \cos[\Omega(t-t')] f(t') = 0$$

and we can easily show that this fixes low Fourier components of $f(t)$ but leaves higher ones open.

The situation changes, if we impose, e.g., an energetic constraint to the control. This typically leads to constraints of the form

$$\int_0^T dt f^2(t) = \int_{-\infty}^{\infty} d\omega f(\omega) f^*(\omega) \leq A$$

where A is the imposed maximum and we have used symmetry properties of the Fourier transform of real-valued functions. Thus, the sum of Fourier components needs to be bounded and if the constraint is too close, there may not even be any solution. This is an example showing that constraints clearly influence the number of accessible solutions and their potential performance, which is commonly seen in practice.

2.2 Optimal control for a classical system

The previous section hinged on having a closed-form Green's function solution of the equation of motion, which is not always available. This follows chapter 2.3 of Bryson and Ho [6].

Suppose we have a dynamical system that can be controlled by a control parameter u that enters a dynamic equation for the state variable x in the form

$$\dot{x} = f[x(t), u(t), t] \quad 0 \leq t \leq T \quad (1)$$

with a given $x(0)$. Both x and u can be single variables or vectors of variables. We wish to optimize a cost function at the end of the process $J[x(T), T]$. We recall classical Lagrangian mechanics and introduce a Lagrange multiplier function λ and can thus state based on the constrained calculus of variations that we need to find a stationary point of

$$\bar{J} = J[x(T), T] + \int_0^T dt \lambda^T(t) (f[x(t), u(t), t] - \dot{x})$$

where we have allowed for the complex of coupled equations and thus vector-valued Lagrange multipliers.

The introduction of the Lagrange multiplier allows for the optimization of J , while satisfying the equation of motion (1) at specified times. As such, this means λ has to be time-dependent as well.

We introduce the associated Hamilton's function (which has a similar mathematical origin in the calculus of variations as the Hamiltonians of mechanics yet a very different physical motivation)

$$H[x(t), u(t), \lambda(t), t] = \lambda^T(t) f[x(t), u(t), t] \quad (2)$$

and rewrite our constrained cost function by integrating the last term by parts

$$\bar{J} = J[x(T), T] + \lambda^T(T)x(T) - \lambda^T(0)x(0) + \int_0^T dt \left\{ H[x(t), u(t), \lambda(t), t] + \dot{\lambda}^T x(t) \right\}.$$

Now let's consider the variation in \bar{J} based on variations in $u(t)$ recalling that the times as well as the initial state variable are given. We find

$$\delta\bar{J} = \left(\frac{\partial J}{\partial x} - \lambda^T\right) \delta x \Big|_{t=T} + \lambda^T \delta x \Big|_{t=0} + \int_0^T dt \left[\left(\frac{\partial H}{\partial x} + \dot{\lambda}^T\right) \delta x + \frac{\partial H}{\partial u} \delta u \right].$$

Note that in general we choose the variation at the beginning to be $\delta x(0) = 0$, since we know the exact initial state of the dynamics.

Now the variations of x and u are not independent, they are linked by the equation of motion. Were we not to work with the Lagrange multiplier, we would need to tediously solve the equation of motion for different control functions and then work out how these variations are related. Fortunately, the Lagrange multiplier method allows us to circumvent that problem. Our goal is for $\delta\bar{J}$ to vanish to first order. Choosing a specific Lagrange multiplier to realize this, we finally arrive at

$$\dot{\lambda}^T = -\frac{\partial H}{\partial x} = -\lambda^T \frac{\partial f}{\partial x} \quad \lambda^T(t_f) = \frac{\partial J}{\partial x(t_f)}. \quad (3)$$

These are the Euler-Lagrange equations pertaining to the system. That being satisfied, we are left with the total variation

$$\delta\bar{J} = \underbrace{\lambda^T(0)\delta x(0)}_{=0} + \int_0^T dt \frac{\partial H}{\partial u} \delta u$$

For an extremum to be reached under any variation of the control, we need

$$\frac{\partial H}{\partial u} = \lambda^T \frac{\partial f}{\partial u} = 0 \quad 0 \leq t \leq T. \quad (4)$$

We have shown the ingredients to what can be formalized as the Pontryagin Maximum Principle (PMP). More pragmatically, these equations give us a recipe on how to solve the thus formulated optimal control problem by a coupled gradient search: From a suitable initial guess for $u(t)$

1. Solve the equation of motion eq. (1) to find $x(t)$ using the initial value $x(0)$ that is part of the control problem
2. Find the Lagrange multiplier by solving eq. (3). Note that there is a definite value given at the *end* time T , i.e., we have a final value problem – that is solved like an initial value problem but propagating backwards in time. This back-propagation is typical when we consider this cost functional.
3. With these, compute the effective gradient in eq. (4) and update the values of u following the direction of the gradient. Adjust the step size as needed.

Iterating these three steps will get us to a local solution, depending on the initial conditions, if the control landscape admits one.

2.2.1 Example: Driven harmonic oscillator

Let us get back to formulating these steps for the optimal control problem of the driven harmonic oscillator described above in section 2.1. We identify the control as the dimensionless force $u \equiv f$ and write the equation of motion as a coupled system

$$\begin{aligned}\frac{dx}{dt} &= \dot{x} \\ \frac{d\dot{x}}{dt} &= -\Omega^2 x + u \\ x(0) &= 0 \quad \dot{x}(0) = 0\end{aligned}$$

In order to have a differentiable performance index that forces the particle to end at a at time T and in rest we can write

$$J = \Omega^2 (x - a)^2 + \dot{x}^2. \quad (5)$$

This leads us to Hamilton's function following the prescription of 2

$$H = \lambda_1 \dot{x} + \lambda_2 (u - \Omega^2 x).$$

So the Euler-Lagrange equations 3 describing the Lagrange Multiplier

$$\dot{\lambda}_1 = \lambda_2 \Omega^2 \quad \dot{\lambda}_2 = -\lambda_1 \quad (6)$$

which remarkably describes a free harmonic oscillator. It is such interpretations that lead to the Lagrange multiplier to be called the adjoint system. The final conditions from eq. (3) are

$$\lambda_1(T) = 2\Omega^2(x(T) - a) \quad \lambda_2(T) = 2\dot{x}(T) \quad (7)$$

which are of course both zero if the final conditions are met (thus, for the optimal solution, the adjoint system vanishes at T). The gradient flow for the control is given by eq. (4)

$$\frac{\partial H}{\partial u} = \lambda_2.$$

Again, iterating these equations will give us a suitable control.

We could guess as a first control that $u_0(t) = \Omega^2 a$ (which is the force needed to keep the particle at rest at the final position, so at least a motivated guess) thus leading to the equation of motion

$$\ddot{x}_0 + \Omega^2(x_0 - a) = 0$$

with the solution $x_0(t) = a(1 - \cos \Omega t)$ and thus $\dot{x}_0 = a\Omega \sin \Omega t$. This clearly does not solve the control problem, we have from eq. (5) $J = \Omega^2 a^2$. In fact, the final conditions eq. 7 for the adjoint system are $\lambda_1(T) = -2\Omega^2 a \cos \Omega T$ and $\lambda_2(T) = 2a\Omega \sin \Omega T$ leading us, by solving eq. (6)

$$\begin{aligned}\lambda_1 &= -2\Omega^2 a \cos \Omega T \cos [\Omega(t - T)] + 2a\Omega^2 \sin \Omega T \sin [\Omega(t - T)] \\ &= -2a\Omega^2 \cos \Omega t\end{aligned}$$

and $\lambda_2 = -2 \sin \Omega t$. This means that the gradient suggests introducing a resonant drive – as we have seen from the exact solution above.

For further treatment of the classical Harmonic oscillator, see [3].

2.3 Gradient-based optimal quantum control with the GRAPE algorithm

These principles can be transferred to the control of quantum systems in a straightforward way. This is easily illustrated with the Gradient Ascent Pulse Engineering (GRAPE) algorithm [29].

2.3.1 State-to-state control

We start with a simple state preparation problem. Suppose WLOG that our system is described by a Hamiltonian

$$\hat{H}(t) = \hat{H}_0 + \sum_{i=1}^n u_i(t) \hat{H}_i.$$

We call the time-independent part of the Hamiltonian \hat{H}_0 the drift, the fields u_i are the controls and \hat{H}_i are the control Hamiltonians. In atomic physics, say, \hat{H}_0 describes the energy level structure of the atom, u_i are laser or microwave fields and \hat{H}_i are dipole operators describing the different field modes including polarization. Our task is now to start at an initial state $|\psi_0\rangle$ at time $t = 0$ and find controls such that we reach state $|\psi_1\rangle$ at time $t = T$. As in quantum physics the global phase is meaningless, this corresponds to maximizing the overlap $J = |\langle \psi_1 | \psi(T) \rangle|^2$. The dynamics of our system is, of course, subject to the Schrödinger equation

$$i\hbar\partial_t|\psi(t)\rangle = \hat{H}(t)|\psi(t)\rangle.$$

Mathematically we got ourselves a system of the exact same structure as the previous one. We give its derivation in the form of Ref. [29].

Many practical generators for u_i such as standard arbitrary wave form generators (AWGs or Arbs) used in superconducting qubits represent² the pulse in a piecewise constant fashion, so it is natural³ to represent the $u_i(t)$ in that same way: We chop the total time into N intervals of length $\delta t = T/N$ and write

$$u_i(t) = u_i(j) \quad \text{for} \quad (j-1)\delta t \leq t < j\delta t.$$

This allows us to write down the formal solution of the Schrödinger equation as

$$\hat{U}(T) = \hat{U}_N \hat{U}_{N-1} \cdots \hat{U}_2 \hat{U}_1$$

with

$$\hat{U}_k = \exp\left(-\frac{i}{\hbar}\delta t \left(\hat{H}_0 + \sum_i u_i(j)\hat{H}_i\right)\right) \quad (8)$$

which we can introduce into the performance index as

$$J = \left|\langle \psi_1 | \hat{U}(T) \psi_0 \rangle\right|^2 = \left|\langle \psi_1 | \hat{U}_N \cdots \hat{U}_1 \psi_0 \rangle\right|^2.$$

We are at liberty to move some of the factors into the adjoint state, giving us

$$J = \left|\langle U_{m+1}^\dagger \cdots U_N^\dagger \psi_1 | \hat{U}_m \cdots \hat{U}_1 \psi_0 \rangle\right|^2$$

² but not necessarily output, as the output is typically smoothed and filtered

³ although not always optimal, see below

or $J = |\langle \lambda_m | \rho_m \rangle|^2$ with $|\rho_m\rangle = \hat{U}_m \cdots \hat{U}_1 |\psi_0\rangle$ $|\lambda_m\rangle = \hat{U}_N \cdots \hat{U}_{m+1} |\psi_1\rangle$. Here, the partially propagated state $|\rho_m(t)\rangle$ is overlapped with the partially back-propagated adjoint state $|\lambda_m(t)\rangle$ – both states are overlapped at time t_m . We thus sweep the time at which we calculate the overlap based on the actual pulse that we apply. Now the final ingredient we need is the derivative of an exponential proven in Theorem 4.5 of [23] (see also [24])

$$\left. \frac{d}{dt} \right|_{t=0} e^{X+tY} = e^X \left\{ Y - \frac{[X, Y]}{2!} + \frac{[X, [X, Y]]}{3!} - \dots \right\} \quad (9)$$

Both of these together allow us to determine all the gradients needed to compute an update at any time step as shown in the left column of figure 1.

We can rewrite this as

$$\left. \frac{d}{dt} \right|_{t=0} e^{X+tY} = e^X \int_0^1 d\tau e^{\tau X} Y e^{-\tau X}$$

by simple power counting. This allows us to analytically compute the derivative of the propagator across one time step by identifying $\hat{X} = \hat{H}(t)$ (the Hamiltonian including the current values of the control) and $\hat{Y} = \hat{H}_i$, one of the control Hamiltonians. In order to simplify the right-hand side, we define $\hat{U}_k(j) = \hat{U}_k^j$ (taking the exponential here simply means to stretch time and study the integral on the right

$$\begin{aligned} & \int_0^1 d\tau \hat{U}_k(j) \hat{H}_i \hat{U}_k^\dagger(j) \\ &= \int d\tau \left(1 - i\tau \delta_t \hat{H} - \tau^2 \delta_t^2 \hat{H}^2 + \dots \right) \hat{H}_i \left(1 + i\tau \delta_t \hat{H} - \tau^2 \delta_t^2 \hat{H}^2 + \dots \right) \\ &= \int d\tau \left(\hat{H}_i - i\tau \delta_t [\hat{H}, \hat{H}_i] + \dots \right) \\ &\simeq \hat{H}_i \end{aligned}$$

where we assume that the time steps chosen are so small that the integral over the commutator can be neglected⁴. A self-contained derivation is presented later in 2.5.4. Restoring all the units leads us to the closed gradient formula

$$\frac{\partial J}{\partial u_i(j)} = -i\delta_t \langle \lambda_j | \hat{H}_i | \rho_j \rangle \quad (10)$$

meaning that we can expect, with an appropriate value of ϵ compute a gradient-based update

$$u_i(j) \mapsto u_i(j) + \epsilon \frac{\partial J}{\partial u_i(j)} \quad (11)$$

This allows us to extremalize J hence to find controls that best approximate the final state with the following algorithm. Starting from an initial guess for the controls:

1. Compute the propagated initial state $|\rho_m\rangle = \hat{U}_m \cdots \hat{U}_1 |\psi_0\rangle$ for all $m \leq N$ by iterative matrix multiplication.

⁴ we will later, under the Magnus expansion, study related steps more carefully

2. Compute the back-propagated final state $|\lambda_m\rangle = \hat{U}_N \cdots \hat{U}_{m+1} |\psi_1\rangle$ by iterative matrix multiplication
3. Compute the gradient of the performance index and update the controls following eqs. (10), (11)
4. Iterate until the value of J is satisfactory or the updates are below a threshold

There are a lot of practical improvements that were found beyond this which we will describe below.

One must not underestimate the importance of this analytical derivation of a gradient. Whenever a gradient is available, it greatly improves the convergence of a search specifically when going from a rough initial guess that can often be obtained by solving an approximate version of the problem at hand to a solution that has the very high precision generally demanded by quantum technologies. If a gradient is available, its analytical and exact derivation is also paramount – numerical gradients are very hard to control numerically as they involve a small difference between two potentially large numbers. In pioneering, pre-GRAPE work [47] this was rather obvious – even with large computational effort, only few parameters could be optimized.

2.3.2 An alternative, direct derivation

An alternative derivation of the variational approach to quantum optimal control is as follows:

Let us again look at the state transfer task. We shall construct a functional, J , to be maximized, and utilize Lagrange multipliers to enforce both the initial condition and the equation of motion. We shall parameterize our control fields, $u(t)$ using a vector of scalar real parameters $\vec{\alpha}$.

Our aim is to maximize the overlap of the goal state $|\psi_{\text{goal}}\rangle$ and the state at final time T , $|\psi(T)\rangle$,

$$J_{\text{goal}} = |\langle \psi(T) | \psi_{\text{goal}} \rangle|^2. \quad (12)$$

We need to impose an initial condition, utilizing a Lagrange multiplier λ_{init}

$$J_{\text{init}} = \lambda_{\text{init}} (|\langle \psi(0) | \psi_{\text{init}} \rangle|^2 - 1). \quad (13)$$

Next, we must guarantee the Schrödinger equation, $(i\hbar\partial_t - H(\vec{\alpha}, t)) |\psi(t)\rangle = 0$ is upheld at all times. To do that, at each point in time, t , we must multiply the equation of motion by the Lagrange multiplier $\langle \chi(t) |$, and we must add the contributions for all points in time:

$$J_{\text{e.o.m}} = \int_0^T \langle \chi(t) | i\hbar\partial_t - H(\vec{\alpha}, t) | \psi(t) \rangle \quad (14)$$

Note that in $J_{\text{e.o.m}}$, $\langle \chi(t) |$ can be interpreted as a conjugate state, propagating backwards in time, as the term can be rewritten as $\langle (-i\hbar\partial_t - H(\vec{\alpha}, t)) \chi(t) | \psi(t) \rangle$.

The functional to be minimized is then

$$J = J_{\text{init}} + J_{\text{e.o.m}} + J_{\text{goal}} \quad (15)$$

We then proceed in the standard variational approach, taking the gradient of this functional with respect to $\bar{\alpha}$ and requiring

$$\partial_{\bar{\alpha}} J = 0. \quad (16)$$

2.3.3 Synthesis of unitary gates

We will now go to the topic of finding controls that best approximate a quantum gate. This can be viewed as a generalization of the state preparation problem to rotating a full basis of the Hilbert space into a desired new basis. This first begs the question of how to find an appropriate performance index. It can be accomplished by starting with a distance measure between the desired and the actual final unitary $\left\| \hat{U}_{\text{target}} - \hat{U}(T) \right\|$. The most common choice is based on the 2-norm

$$\begin{aligned} \left\| \hat{U}_{\text{target}} - \hat{U}(T) \right\|_2^2 &= \text{Tr} \left[\left(\hat{U}_{\text{target}}^\dagger - \hat{U}^\dagger(T) \right) \left(\hat{U}_{\text{target}} - \hat{U}(T) \right) \right] \\ &= \text{Tr} \left[\hat{U}_{\text{target}}^\dagger \hat{U}_{\text{target}} + \hat{U}^\dagger(T) \hat{U}(T) - \hat{U}_{\text{target}}^\dagger \hat{U}(T) - \hat{U}^\dagger(T) \hat{U}_{\text{target}} \right] \\ &= 2 \left(d - \text{ReTr} \hat{U}_{\text{target}}^\dagger \hat{U}(T) \right) \end{aligned}$$

where d is the underlying Hilbert space dimension. Thus, we see that minimizing the error corresponds to maximizing the overlap $\text{ReTr} \hat{U}_{\text{target}}^\dagger \hat{U}(T)$.

Now the real part looks suspicious – if we have the gate right up to a global phase, $\hat{U}(T) = e^{i\phi} \hat{U}_{\text{target}}$ this overlap indicates a non-perfect result. In fact, numerical experimentation shows that this would be a serious drawback. We can trace this error back to the original distance measure. The high-brow step to take now would be to elevate the description to full quantum channels. Pragmatically, we move from real part to absolute square and thus the most common performance index for gates is

$$J = \left| \text{Tr} \left(\hat{U}_{\text{target}}^\dagger \hat{U}(T) \right) \right|^2.$$

This quantity can be interpreted in a somewhat operational fashion: First apply the gate you have, then undo the gate you want. If everything goes right you have but a global phase – the same one on all vectors of the standard basis. If not, you measure the deviation from unity for the complete standard basis. There are other possible choices (and good reasons to think about them), which we will discuss later. With this quantity, we can proceed in a way similar to state transfer, only that now we of course start at the unit matrix. We again use piecewise constant controls and define both the intermediate propagator and the intermediate back-propagated target

$$\hat{X}_j = \hat{U}_j \cdots \hat{U}_1 \quad \hat{P}_j = \hat{U}_{j+1}^\dagger \cdots \hat{U}_N^\dagger \hat{U}_{\text{target}}$$

allowing us to rewrite $J = \left| \text{Tr} \hat{P}_j^\dagger \hat{X}_j \right|^2$ for all values of j . We can now apply the same identities

as before and find

$$\begin{aligned} \frac{\partial J}{\partial u_i(j)} &= \frac{\partial}{\partial u_i(j)} \left(\text{Tr} \hat{P}_j^\dagger \hat{X}_j \right) \left(\text{Tr} \hat{P}_j^\dagger \hat{X}_j \right)^* \\ &= 2\text{Re} \left[\left(\frac{\partial}{\partial u_i(j)} \text{Tr} \hat{P}_j^\dagger \hat{X}_j \right) \left(\text{Tr} \hat{P}_j^\dagger \hat{X}_j \right) \right] \\ &= -2i\delta t \text{Re} \left[\left(\text{Tr} \hat{P}_j^\dagger \hat{H}_i \hat{X}_j \right) \left(\text{Tr} \hat{P}_j^\dagger \hat{X}_j \right) \right]. \end{aligned}$$

With this analytical gradient, the GRAPE algorithm can be applied as above.

2.4 The Krotov algorithms

The Krotov algorithm [33, 34, 51, 55] has been formulated before the GRAPE algorithm. Some of its presentations are historically based on applications in chemistry and emphasizes constraints more than its core. Looking back on how GRAPE is applied, we are blessed with an analytical gradient formula which in each iteration allows us to calculate the gradient of the cost function(al) with respect to all controls at all times and then by walking against it look for improved controls. Notably, the gradient is always computed at a point in parameter space given by the controls computed in the *previous* iteration.

There are two different algorithms which carry the name ‘‘Krotov’’ - a fact which can be quite confusing, even for experts in the field.

The first Krotov, prides itself with its monotonic convergence, which is achieved by propagating the forward state using the old control field, while the backward-propagating state makes use of the new field. A detailed description, with Python implementation, can be found in [21].

The second Krotov can be considered a greedy version of GRAPE, and is described in detail in [41]: In this version of the Krotov algorithm, all previously computed knowledge is used, i.e., once an entry to the gradient is computed, it is applied right away and the next element of the gradient is computed with that correction already applied. This approach of not leaving any information behind in general lowers the number of iterations needed to reach convergence and it comes with proven monotonic convergence. On the other hand, each iteration step takes more time.

The various update strategies are visualized in figure 1.

Benchmarking of the various optimal control algorithms is a topic of ongoing research.

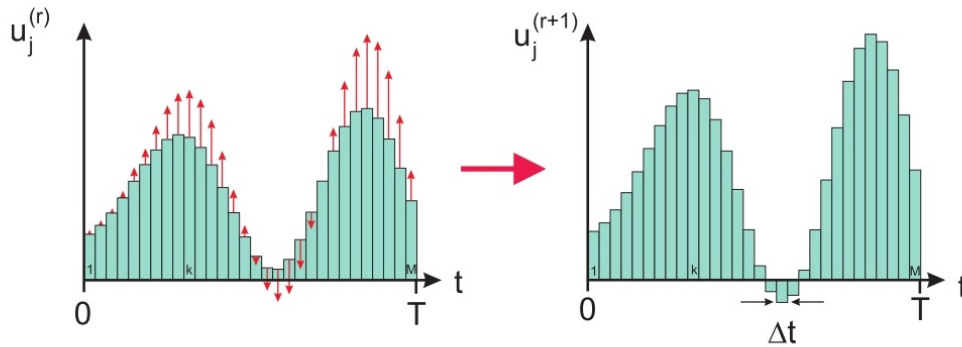
2.5 Modern numerical issues

2.5.1 Control landscapes

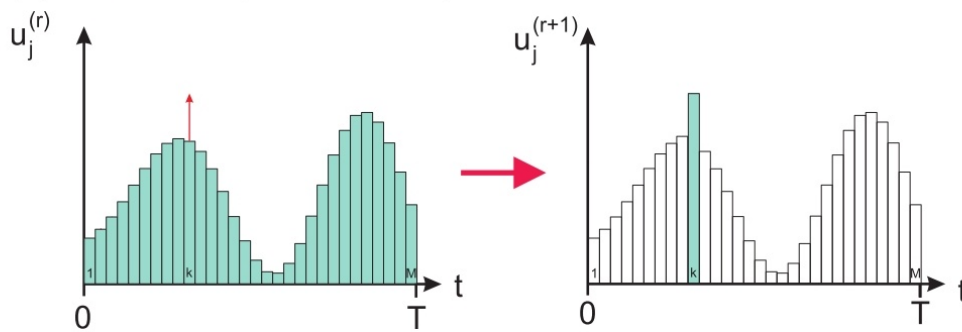
A gradient search with an analytical gradient as outlined is the best way to find a local extremum of an optimization landscape. If the optimization landscape has multiple local minima, it can get stuck in a local minimum and needs to be enhanced.

In a seminal series of papers, Rabitz has shown (see e.g. [52]) that there is indeed only one extremum in the control landscape and that it is global. This theorem is a correct derivation of

(a) concurrent (GRAPE-type)



(b) sequential (Krotov-type)



(c) hybrid

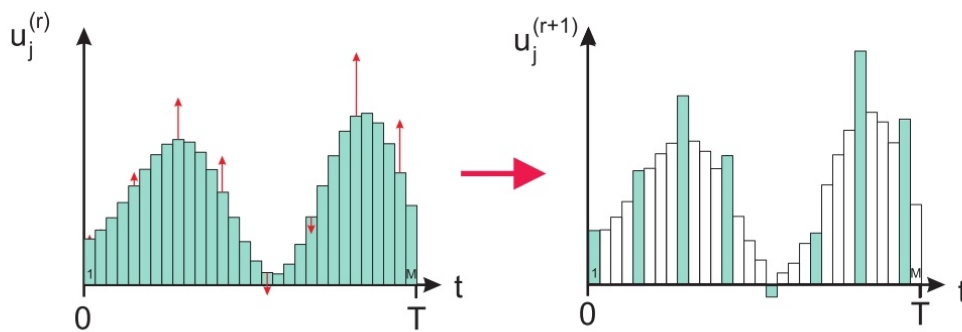


Figure 1: Overview on the update schemes of gradient-based optimal control algorithms in terms of the set of time slices $T(q) = \{k(q), k(q), \dots, k(q)\}$ for which the control amplitudes are concurrently updated in each iteration. Subspaces are enumerated by q , gradient-based steps within each subspace by s , and r is the global step counter. In grape (a) all the M piecewise constant control amplitudes are updated at every step, so $T(1) = \{1, 2, \dots, M\}$ for the single iteration $q \equiv 1$. Sequential update schemes (b) update a single time slice once, in the degenerate inner-loop $s \equiv 1$, before moving to the subsequent time slice in the outer loop, q ; therefore here $T(q) = \{q \bmod M\}$. Hybrid versions (c) follow the same lines: for instance, they are devised such as to update a (sparse or block) subset of p different time slices before moving to the next (disjoint) set of time slices.

its assumptions – one of which is the absence of constraints in pulse amplitude and temporal resolution. In practice, these constraints exist and multiple local extrema exist – the more constrained the optimization, the more local extrema. Specifically in situations close to the quantum speed limit (see below), with low control resolution (Ref [36] looks at a single bit of amplitude resolution and required genetic algorithms to converge) or with complex many-body dynamics and only few controls, these call for more advanced methods.

If one has a good intuition about the optimal pulse say, by solving a model that is very close to the desired model or by rescaling a solution that works at a longer gate duration, one can often stay close to the global extremum and otherwise requires a gradient search. If that is not the case, one needs to first start with a more global search method covering a large parameter space. Known systems for such gradient-free approaches are GROUP [61], genetic algorithms ([27, 36]), they are part of CRAB (see section 3.2) and simulated annealing [65].

2.5.2 Fidelities

We would like to come back to the choice of fidelity based on the 2-norm described above. It has been argued that the most appropriate way to characterize quantum processes is the use of the diamond norm [56]. It can be expressed for a quantum operation \mathcal{E} compared to an ideal operation \mathcal{U} as

$$\|\mathcal{U}_{\text{ideal}} - \mathcal{E}\|_{\diamond} = \sup_q \max_{\psi} |\text{Tr} [\mathcal{U}_{\text{ideal}}(|\psi\rangle\langle\psi|) - \mathcal{E}(|\psi\rangle\langle\psi|)]| \quad (17)$$

This involves two generalizations of the 2-norm: On the one hand, rather than taking the 2-norm distance which is equivalent to averaging over all possible input states to the operation, we are taking the maximum over $|\psi\rangle$, i.e., we choose the input state that maximizes the distance. On the other hand, rather than directly using the unitary operation, we enhance the Hilbert space by adding another space of dimension q on which the identity operation is performed. The diamond norm is then the supremum over q . The latter may sound rather academic, but it is not if, e.g., the initial state is entangled between the original and the auxiliary system.

For the purposes of quantum optimal control, the diamond norm is rather impractical – it is hard to compute (as it contains a supremum) and it can be non-differentiable (as it contains taking a maximum over states, the state at which it has reached can jump in state space). What does this mean for the applicability of quantum optimal control in the context of fault tolerance?

There are two answers to this question. On the one hand, one can at least find performance indices that emphasize the worst case more strongly while being differentiable. A straightforward option is [26]

$$\begin{aligned} J_q &= \max_{\alpha \in [0, 2\pi)} \left\| \hat{U}_{\text{target}} - e^{i\alpha} \hat{U}(T) \right\|_{2q}^{2q} \\ &= \max_{\alpha \in [0, 2\pi)} \text{Tr} \left[\left(\hat{U}_{\text{target}}^\dagger - e^{-i\alpha} \hat{U}^\dagger(T) \right) \left(\hat{U}_{\text{target}} - e^{i\alpha} \hat{U}(T) \right) \right]^q \end{aligned}$$

which can be implemented in a straightforward fashion yet does not have a known extension that avoids optimizing the global phase.

On the other hand, it is pragmatically not very crucial to go through these steps as long as the algorithm converges properly: Our goal is to get the error as close to zero as possible and,

as these norms can be continuously mapped onto each other, one pragmatically searches for controls that reduce the error in the 2-norm to an extremely low value which guarantees that even in the desired norm the error is low enough – using the paradigm to control and verify with two different measures.

2.5.3 Increasing precision of GRAPE

The GRAPE algorithm above defines a straightforward gradient algorithm for optimal control. There are a few known measures to speed up its convergence.

One measure is the improvement of the use of the gradient by moving to a quasi-Newton method, the Broyden, Fletcher, Goldfarb, and Shanno (BFGS) method [48]. Newton’s method, as the reader may have learned in an elementary introduction to numerical mathematics, rely on approximating the function whose zero we desire to find by its tangent – in our case, we desire to find the zero of the gradient, i.e., we need to approximate the functions up to its second derivative. As we are optimizing a scalar that depends on many parameters – all the controls taken at all the times of interest – the matrix of second derivatives is a high-dimensional object. In order to approximate the zero of the gradient, one would have to invert that matrix, which is numerically hard and would likely negate the potential computational advantage. The BFGS method instead relies on directly approximating the inverse Hessian

2.5.4 The gradient of a matrix exponential

Expanding on the discussion surrounding eq. (8), (9), any gradient-driven optimal control optimization, such as GRAPE or Krotov, which treats the control fields as piecewise constant, will describe the coherent propagator of time slice m as

$$U_m = \exp\left(-\frac{i}{\hbar}\delta_t H(\bar{\alpha}, t_m)\right) \quad (18)$$

where $\bar{\alpha}$ parameterizes the control functions $u(t)$. We are searching for the value of $\bar{\alpha}$ which will minimize the infidelity. At step j of the optimization, to compute the gradient of the goal function with respect to $\bar{\alpha}$, we must compute $\partial_{\bar{\alpha}} U_m(\bar{\alpha})|_{\bar{\alpha}=\bar{\alpha}_j}$. At this point we can rewrite eq. (18) as in eq. (9),

$$U_m = \exp\left(-\frac{i}{\hbar}\delta_t \left(H_{m,j} + \epsilon_{\bar{\alpha}} \tilde{H}_{m,j}\right)\right)$$

where $\epsilon_{\bar{\alpha}}$ is small and we seek $\partial_{\epsilon_{\bar{\alpha}}} U_m(\epsilon_{\bar{\alpha}})|_{\epsilon_{\bar{\alpha}}=0}$. Following [2, 35], and their summary in Appendix A of [41], we denote the eigenvalues and eigenvectors of H_j by e_k and $|e_k\rangle$, respectively, then using the spectral theorem

$$\langle e_l | \partial_{\epsilon_{\bar{\alpha}}} U_m | e_k \rangle = \begin{cases} -\frac{i}{\hbar}\delta_t \langle e_l | \tilde{H}_{m,j} | e_k \rangle \exp\left(-\frac{i}{\hbar}\delta_t e_l\right) & \text{if } e_l = e_k \\ -\frac{i}{\hbar}\delta_t \langle e_l | \tilde{H}_{m,j} | e_k \rangle \frac{\exp\left(-\frac{i}{\hbar}\delta_t e_l\right) - \exp\left(-\frac{i}{\hbar}\delta_t e_k\right)}{-\frac{i}{\hbar}\delta_t (e_l - e_m)} & \text{if } e_l \neq e_k \end{cases}$$

one may invoke the spectral theorem in a standard way and calculate matrix functions via the eigendecomposition.

To simplify notation, we shall look at $\partial_x e^{A+xB}$, with A, B being an arbitrary pair of Hermitian (non-commuting) matrices and $x \in \mathbb{R}$. As previously $\{|e_l\rangle\}$ as the orthonormal eigenvectors to the eigenvalues $\{e_l\}$ of A . We then obtain the following straightforward, if somewhat lengthy, derivation:

$$\begin{aligned}
 D &= \left\langle e_l \left| \partial_x e^{A+xB} \right| e_k \right\rangle \Big|_{x=0} \\
 &= \left\langle e_l \left| \partial_x \sum_{n=0}^{\infty} \frac{1}{n!} (A+xB)^n \right| e_k \right\rangle \Big|_{x=0} \\
 &= \left\langle e_l \left| \sum_{n=0}^{\infty} \frac{1}{n!} \sum_{q=1}^n (A+xB)^{q-1} B (A+xB)^{n-q} \right| e_k \right\rangle \Big|_{x=0} \\
 &= \left\langle e_l \left| \sum_{n=0}^{\infty} \frac{1}{n!} \sum_{q=1}^n A^{q-1} B A^{n-q} \right| e_k \right\rangle \\
 &= \sum_{n=0}^{\infty} \frac{1}{n!} \sum_{q=1}^n e_l^{q-1} \langle e_l | B | e_k \rangle e_k^{n-q} \\
 &= \langle e_l | B | e_k \rangle \sum_{n=0}^{\infty} \frac{1}{n!} \sum_{q=1}^n e_l^{q-1} e_k^{n-q}
 \end{aligned}$$

This provides the answer for in the case where $e_l = e_k$. For $e_l \neq e_k$ a bit more work is needed:

$$\begin{aligned}
 D &= \langle e_l | B | e_k \rangle \sum_{n=0}^{\infty} \frac{1}{n!} e_k^{n-1} \sum_{q=1}^n \left(\frac{e_l}{e_k} \right)^{q-1} \\
 &= \langle e_l | B | e_k \rangle \sum_{n=0}^{\infty} \frac{1}{n!} e_k^{n-1} \frac{(e_l/e_k)^n - 1}{(e_l/e_k) - 1} \\
 &= \langle e_l | B | e_k \rangle \sum_{n=0}^{\infty} \frac{1}{n!} \frac{e_l^n - e_k^n}{e_l - e_k} \\
 &= \langle e_l | B | e_k \rangle \frac{e^{e_l} - e^{e_k}}{e_l - e_k}
 \end{aligned}$$

Note that we have explicitly made use of the orthogonality of eigenvectors to different eigenvalues in normal matrices.

3 Applied optimal quantum control

While quantum optimal control is a well-developed field and has been very successful in atomic and molecular systems, its track record in solid-state quantum technologies is somewhat less developed. The reason has to do with the accuracy of the models, i.e., the precision at which we know every ingredient of the Hamiltonian. First of all, a quantum-technological device

(specifically, but not exclusively, in the solid state) has human-made components which contain some fabrication uncertainty. This affects the drift Hamiltonian – even if its eigenvalues can be accurately determined using spectroscopy, it is much more involved to find its eigenvectors. These naturally also affect the matrix elements of the control Hamiltonians. On top of that, some solid-state quantum devices need to be extremely well isolated from their environments including high-temperature black-body radiation. This means, that an applied control signal will get distorted on its way to the sample in a way that can be measured only to a limited degree, see fig. 2 for a summary. While one can improve hardware and characterization to meet these challenges, it is hard to get this to the precision required by, say, fault-tolerant quantum computing. Thus, other approaches are called for.

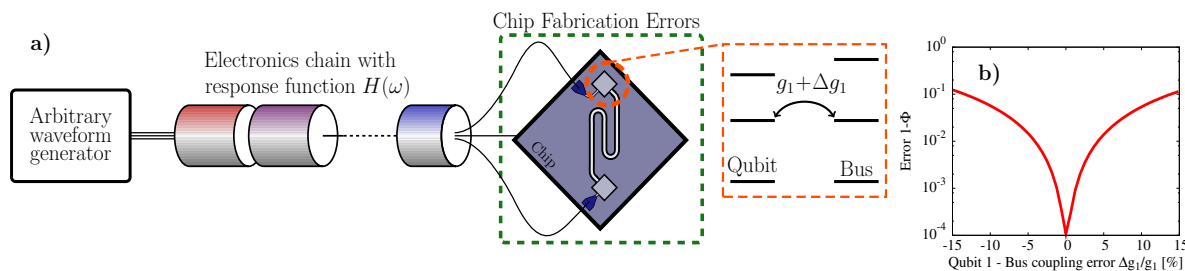


Figure 2: Typical sources of inaccuracy in quantum control for superconducting qubits including the transmission from the generator to the sample and inaccuracy of the Hamiltonian model. Right: Typical error sensitivity for a gate between superconducting qubits.

3.1 Closing the loop for pulse calibration

One possible approach to handle uncertainties would be to use a robust control methodology inspired by magnetic resonance in ensembles. While this method can be useful, it slightly misses the point: It still requires a good estimate for the uncertainty and then it improves performance across the relevant parameter interval. Here, the situation is different, we do not have a parameter distribution but a single set of parameters – we just cannot find it or even the relevant model *a priori*.

One way to still find good pulses are hybrid control methods such as Adaptive Hybrid Optimal Control (AdHOC, [14]), Optimized Randomized Benchmarking for Immediate Tuneup (ORBIT, [28]), and Adaptive Control via Randomized Optimization Nearly Yielding Maximization (ACRONYM, [16]). The idea of these methods is rather similar: After an initial design phase that may or may not contain traditional optimal control, a set of pulses is constructed based on models that are believed to approximate the actual system but its parameterization is left open to some corrections. These corrections are then determined in a closed loop – the fidelity is measured and the pulses are updated based on these fidelity measurements.

In the example of AdHOC, the pulse measurement is based on randomized benchmarking (described below) and the optimization that determines the corrections is based on the Nelder-Mead simplex algorithm, which is available in most numerical mathematics toolboxes. What is crucial is that this is a gradient-free algorithm in order to avoid issues with taking gradients of measurement data. Is that as a simplex algorithm, the search for a pulse described by n parameters needs to be initialized using $n + 1$ initial guesses. This raises the important question how the

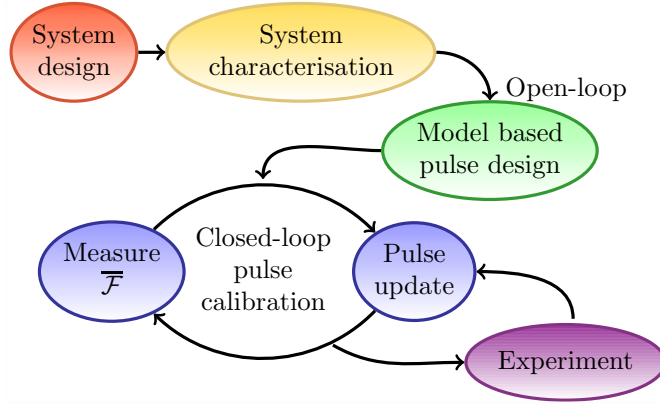


Figure 3: Typical two-stage control workflow with an open loop modeling stage

number n can be kept as small as possible (but not smaller, see below) by finding an efficient parameterization.

This is not an easy problem. So far, we have always assumed that the pulses are parameterized in piecewise constant fashion and have argued that this is naturally compatible with arbitrary wave form generators. However, this parameterization does not naturally lend itself to reduction of the number of parameters – simple, sparse controls in quantum physics are typically sine and cosine functions with smooth, Gaussian-derived envelopes. On the other hand, the piecewise constant parameterization was instrumental in deriving the gradient formula in an analytical way and cannot be easily removed.

3.2 CRAB

Albeit originally developed from a different motivation, the optimization of many-body dynamics, the Chopped RANdom Basis (CRAB)⁵ algorithm serves that purpose, [13]. It introduced the concept of simple and sparse pulse parameterizations, i.e., finding a pulse parameterization that is not necessarily piecewise constant but rather can be written as

$$H(\bar{\alpha}, t) = H_0 + \sum_{k=1}^C c_k(\bar{\alpha}, t) H_k, \quad (19)$$

where the functions c_k can e.g. be harmonic functions characterized by amplitude, frequency and phase or a sequence of Gaussians

$$c_k(\bar{\alpha}, t) = \sum_{j=1}^m A_{k,j} \exp\left(-\frac{(t - \tau_{k,j})^2}{\sigma_{k,j}^2}\right). \quad (20)$$

In complex systems that were the initial motivation for CRAB, one has very little prior knowledge about a suitable basis and it is at best chosen random, hence the name. CRAB utilizes a gradient-free search, specifically Nelder-Mead (although other algorithms could be used), similarly to what we have already described for AdHOC⁶.

⁵ pronounced with a rolling 'r' and a voiced 'b'

⁶ note that CRAB was proposed before AdHOC

The fact CRAB is model-free, with the gradient-free search treating the quantity to be optimized as a black box, provides a distinct advantage in situations a precise model is unknown or when the model is known, but the gradient cannot be computed due to numerical complexity or other reasons. This makes CRAB appropriate for closed-loop experimental calibration of control fields in systems ranging from nitrogen vacancy centers in nano-diamonds [5] and cancer treatment formulations [4], to DMRG-based simulations [59]. Further, CRAB enjoys huge success in studying quantum phase transitions, preparing large Schrödinger cat states, sensing and many more.

A variant of CRAB, known as dCRAB [53], deals with a situation where the control parameterization has a higher dimensionality than can be optimized by Nelder-Mead, by iteratively optimizing different subsets (or low-dimension projections) of the high-dimension full parameter space.

3.3 GOAT

Gradient Optimization of Analytic conTrols (GOAT) is a recently [40] proposed optimal control algorithm which does not derive from the variational formulation of optimal control, defined earlier. Rather, GOAT finds the equations of motion for the gradient of the goal function with respect to the control parameters, integrating as you would the Schrödinger equation (as piecewise-constant approximation, or using standard ODE tools such as Runge-Kutta optimizers).

For our purpose, the goal function to minimize is defined as the projective SU distance (infidelity) between the desired gate, U_{goal} , and the implemented gate, $U(T)$, [49] (also [62])

$$g(\bar{\alpha}) := 1 - \frac{1}{\dim(U)} \left| \text{Tr} \left(U_{\text{goal}}^\dagger U(T) \right) \right|, \quad (21)$$

where $U(t)$ is the time ordered (\mathbb{T}) evolution operator

$$U(\bar{\alpha}, T) = \mathbb{T} \exp \left(\int_0^T -\frac{i}{\hbar} H(\bar{\alpha}, t) dt \right). \quad (22)$$

GOAT's ability to use any control ansatz makes it feasible to find drive shapes described by a small number of parameters, suitable for closed-loop calibration.

A gradient-based optimal control algorithm requires two ingredients: an efficient computation of $\partial_{\bar{\alpha}} g(\bar{\alpha})$ and a gradient-based search method over parameter space. GOAT presents a novel method for the former, while using any standard algorithm for the latter, such as BFGS.

Consider the gradient of the goal function eq. (21) with respect to $\bar{\alpha}$,

$$\partial_{\bar{\alpha}} g(\bar{\alpha}) = -\text{Re} \left(\frac{g^*}{|g|} \frac{1}{\dim(U)} \text{Tr} \left(U_{\text{goal}}^\dagger \partial_{\bar{\alpha}} U(\bar{\alpha}, T) \right) \right). \quad (23)$$

Neither $U(\bar{\alpha}, T)$ nor $\partial_{\bar{\alpha}} U(\bar{\alpha}, T)$ can be described by closed form expressions. U evolves under the equation of motion $\partial_t U(\bar{\alpha}, t) = -\frac{i}{\hbar} H(\bar{\alpha}, t) U(\bar{\alpha}, t)$. By taking the derivative of the U equation of motion with respect to $\bar{\alpha}$ and swapping derivation order, we arrive at a coupled system of equations of motion for the propagator and its gradient,

$$\partial_t \begin{pmatrix} U \\ \partial_{\bar{\alpha}} U \end{pmatrix} = -\frac{i}{\hbar} \begin{pmatrix} H & 0 \\ \partial_{\bar{\alpha}} H & H \end{pmatrix} \begin{pmatrix} U \\ \partial_{\bar{\alpha}} U \end{pmatrix}. \quad (24)$$

As $\bar{\alpha}$ is a vector, $\partial_{\bar{\alpha}}U$ represents multiple equations of motion, one for each component of $\bar{\alpha}$. $\partial_{\bar{\alpha}}H$ is computed using the chain rule.

GOAT optimization proceeds as follows: Starting at some initial $\bar{\alpha}$ (random or educated guess), initiate a gradient driven search (e.g. L-BFGS [48]) to minimize eq. (21). The search algorithm iterates, requesting evaluation of eqs. (21,23) at various values of $\bar{\alpha}$, and will terminate when the requested infidelity is reached or it fails to improve g further. Evaluation of $g(\bar{\alpha})$, $\partial_{\bar{\alpha}}g(\bar{\alpha})$ requires the values of $U(\bar{\alpha}, T)$ and $\partial_{\bar{\alpha}}U(\bar{\alpha}, T)$. These are computed by numerical forward integration of eq. (24), by any mechanism for integration of ordinary differential equations that is accurate and efficient for time-dependent Hamiltonians, such as adaptive Runge-Kutta. Initial conditions are $U(t=0) = \mathcal{I}$ and $\partial_{\bar{\alpha}}U(t=0) = 0$. Note that no back propagation is required.

Experimental constraints can be easily accommodated in GOAT by mapping the optimization from an unconstrained space to a constrained subspace, and computing the gradient of the goal function using the chain rule. For example, $\bar{\alpha}$ components may be constrained by applying bounding functions, e.g. $\alpha_k \rightarrow \frac{1}{2}(v_{\max} - v_{\min}) \sin(\bar{\alpha}_k) + \frac{1}{2}(v_{\max} + v_{\min})$ which imposes $\alpha_k \in [v_{\min} \dots v_{\max}]$. Amplitude constraints and a smooth start and finish of the control pulse can be enforced by passing the controls through a window function which constrains them to a time-dependent envelope. Gradients for $\partial_{\bar{\alpha}}H$ flow via the chain rule.

3.4 Evaluating fidelity with randomized benchmarking.

The closed-loop approaches mentioned above crucially rely on a measurement of success. While in state-transfer problems, e.g. creating an ordered state quickly or steering a chemical reaction, there may be generic tools to determine this success with a given experimental apparatus. In the case of a quantum gate, this is not so simple. While classic textbooks like first label quantum process tomography, this has a number of drawbacks, and is now replaced by more efficient methods.

3.4.1 The trouble with tomography

To understand this, let's first take a look at quantum state tomography [39]. This is, in a nutshell, the reconstruction of a quantum state (characterized by its density matrix) by performing a complete set of observable measurements. Next to some practical drawbacks having to do with guaranteeing a positive density matrix [50], this is also impractical: A typical quantum device can be read out with a single machine – an electric or optical measurement. Formally this corresponds to measuring in one basis (we will assume that we are dealing with qubits, so recording the expectation value completely characterizes the output distribution). In order to measure a complete set of operators, one has to first perform a basis change in the shape of performing a coherent operation. As this operation itself is prone to error, this will falsify the result. Together with the intrinsic imperfection of the readout device this constitutes measurement error.

From state tomography, it is another step to process tomography, i.e., the reconstruction of a quantum channel – linear map from input to output density matrices – from measured. Formally, one can use the Choi-Jamiolkowski isomorphism [39] map the process matrix of the channel onto the density matrix of a state and treat the problem of process tomography as one of state tomography. Practically, process tomography involves to now measure complete sets of both

initial and final states that undergo the channel. Similar to measurement, also state preparation is usually possible only in one distinct basis – if state preparation is performed by measurement it is the measurement basis, if state preparation is performed via thermalization or optical pumping it is the drift Hamiltonian’s eigenbasis – and it is imperfect – both of these give rise to state preparation errors. Thus, in total, the quantum channel that one would like to characterize is masked by state preparation and measurement (SPAM) errors.

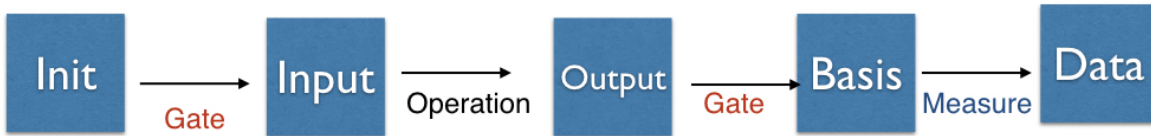


Figure 4: SPAM errors in process tomography: The state that can be prepared and measured needs to be transferred into the basis that has to be prepared and measured, introducing additional errors obfuscating the channel.

On top of that, full process tomography is also forbiddingly labourious. The state of a d dimensional quantum system is characterized by a d^2 entries in a density matrix that, accounting for hermiticity and norm boil down to $d^2 - d + 1$ real numbers. This has to be squared again to describe a quantum channel, leading to $O(d^4)$ numbers – which then are recombined to compute a single fidelity. In an n - Qubit system, we have $d = 2^n$ making full tomography forbiddingly data intensive. On top of that, we would like to ensure complete positivity of the measured channel, which gives rise to inequality constraints that are practically hard to meet specifically when the map is close to unitary. Now there are several methods such as compressed sensing and Monte Carlo sampling [8, 22] that reduce that problem, but with SPAM still included, there is strong motivation to look for an independent method to evaluate fidelity in an experiment. Here, randomized benchmarking and its descendants (RB+) have appeared as a quasi-standard. A comprehensive review of RB+ has currently not been published. We are going to mention key papers on the way and otherwise refer to the work of J. Emerson.

3.4.2 Randomization of quantum channels

Let’s first lay the foundation of how we describe a quantum channel [39]: A linear map that takes any valid density matrix onto another valid density matrix, i.e., with

$$\rho \mapsto \mathcal{E}[\rho]$$

we demand that if ρ is hermitian, positively semidefinite, and has a normalized trace, so is $\mathcal{E}[\rho]$. This is satisfied by the Kraus representation

$$\mathcal{E}[\rho] = \sum_k \hat{A}_k \rho \hat{A}_k^\dagger \quad \sum_k \hat{A}_k^\dagger \hat{A}_k = \mathbb{I}.$$

The (non-unique) *Kraus operators* A_k characterize the channel. It can be easily shown that the Kraus representation leads to a valid channel and it takes a bit more attention to show that the validity of the channel also requires the Kraus representation.

Now to estimate the average fidelity over a channel relative to a desired unitary \hat{U} we apply the channel to a pure initial state, then undo the ideal channel, compute the overlap with the pure state and average over all pure inputs

$$F = \int d\psi \langle \psi | U^\dagger \mathcal{E} [|\psi\rangle\langle\psi| U] | \psi \rangle$$

where the integral runs over a suitable uniform distribution of all states called the Haar measure. We now aim at replacing the average in this formula by another randomization procedure [15]. We now decompose the real operation into an ideal operation followed by an error channel and Kraus-decompose the error channel

$$\mathcal{E} = \Lambda \circ \mathcal{U} \quad \Lambda = \sum_k A_k \rho A_k^\dagger.$$

Plugging this into the expression for the average gets us

$$F = \int d\psi \langle \psi | U^\dagger \Lambda [U |\psi\rangle\langle\psi| U^\dagger] U | \psi \rangle.$$

We can read this expression as implementing the motion-reversal transformation $U^\dagger \cdot U$ with an error Λ occurring in the middle.

Now instead of going for F directly, let us average the fidelity over all unitaries that can enter the motion-reversal map – assuming tacitly that we have the same Λ at all times. We now compute a at first glance very different average – we keep a single initial state $\rho = |\psi\rangle\langle\psi|$ and instead average over all unitaries

$$E = \int dU \text{Tr} [\rho U^\dagger \Lambda (U \rho U^\dagger) U].$$

Now we exchange the order of integration and change the order under the trace and write this as

$$E = \text{Tr} \left(\rho \left[\int dU U \Lambda U^\dagger \right] \rho \right)$$

We can now read this exchanged expression at face value – in the center is noise averaged over all unitaries

$$\Lambda_{\text{ave}} = \int dU U \Lambda U^\dagger.$$

Building on the operations of unitary maps as generalized rotations, this is called a twirled channel. It can be mathematically shown what is physically rather obvious – this channel must be highly symmetric, it cannot prefer any basis over the other. The only channel compatible with this is the depolarizing channel

$$\Lambda_{\text{ave}}[\rho] = p\rho + \frac{1-p}{d}\mathbb{I}$$

which has a single error probability p . With this the error averaged over all unitaries equals the fidelity of the twirled channel computed for a single input state

$$E = \text{Tr}(\rho \Lambda_{\text{ave}} \rho) = F.$$

where the last equality requires some more involved math to show that this is also the same as the average fidelity of a unitary averaged over all states. The fact that a single input state is enough – we have delegated the need for averaging from all states to twirling the channel – addresses the problem of SPAM errors.

Now what is needed is an efficient way to implement Λ_{ave} . We need to replace the integral over all unitaries by a sum over random elements that converges to this integral. This brings in the concept of a unitary 2-design: a set that correctly reproduces the full unitary set in polynomials of degree 2. It can be shown [12, 32] (in a rather pedestrian way) that the Clifford group is sufficient. The Clifford group [39] is formally defined as the normalizer of the Pauli group. For n qubits, this Pauli $P_n = \{\sigma_n\}$ group consists of all direct products of Pauli matrices $\sigma_n = \otimes_{j=1}^n \sigma_{i_j}$, $i_j \in \{0, 1, 2, 3\}$ so the corresponding Clifford group is the set of all unitaries that map all n -qubit Pauli matrices onto Pauli matrices

$$C_n = \{U \in SU(2^n) : \forall \sigma_n \in P_n \exists \sigma_m \in P_m : \sigma_m = U \sigma_n U^\dagger\}.$$

For a single qubit, this group is generated by all quarter-turns around the Bloch sphere. The Clifford group is a discrete group and quantum algorithms consisting of only Clifford gates can be efficiently classically simulated. These together lead to the remarkably simple protocol of randomized benchmarking.

3.4.3 Randomized Benchmarking

Let's pull all of these ingredients together into a handy protocol:

1. Repeat for a few representative sequences
 - (a) Draw a random set of Clifford gates
 - (b) Compute the resulting operation and its inverse. Add the inverse to the end of the sequence
 - (c) Repeat the following to establish an estimate for the final probability for survival of the initial state
 - i. initialize the system in a convenient state
 - ii. run the sequence
 - iii. measure if the outcome is the same state or not
 - (d) Average to estimate the survival probability for the given sequence
2. Average to estimate the survival probability averaged of the Clifford groups. As a function of sequence length, the result will have the form

$$p(n) = p_0 + \lambda^n.$$

Here, λ is the average Clifford gate fidelity and can be determined by fitting, whereas p_0 is the SPAM error.

It turns out practically and can be reasoned analytically that the need for averaging is acceptable, artifacts of ensemble sizes vanish quickly [9].

In this basic version of RB, there are a lot of assumptions that can be questioned. The theory of randomized benchmarking has been extended to adapt most of the demands resulting from weakening these assumptions. We cannot do the vast literature full justice here but mention a few highlights.

First of all, standard RB finds the fidelity averaged over the whole Clifford group. If one instead desires to characterize a single Clifford gate, the technique of interleaved randomized benchmarking (IRB) [42] can be applied. There, one first performs regular RB. Then, one takes the sequences used for RB and interleaves the desired Clifford gate between any two of the gates from the sequence. The inverse to the resulting sequence needs to be re-computed. The comparison between the interleaved and the regular frequencies gives the average fidelity of that special Clifford gate.

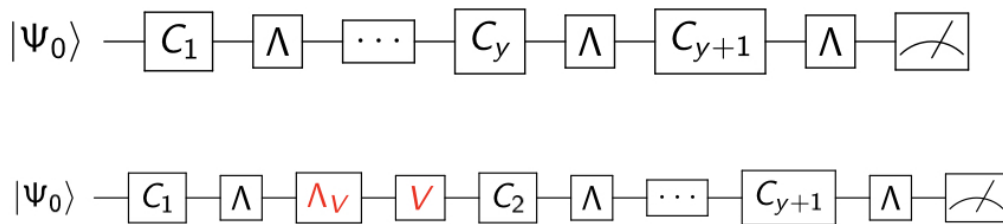


Figure 5: Quantum channels for randomized benchmarking. Top: Randomized Benchmarking consists of a sequence of random (perfect) Clifford C_i and Errors Λ inverted by the last Clifford gate C_{y+1} . Bottom: Interleaved randomized Benchmarking interleaves a particular Clifford gate V into this sequence.

In a similar vein, issues like leakage out of the computational subspace, gate-dependent error and others can be taken into account [9], leading to the modern concept of cycle benchmarking. Including non-Clifford gates, however, can only be done at the cost of significant overhead, as the inverting operation is hard to compute as well as hard to invert - it is an arbitrarily quantum gate encompassing the whole system and not part of the Clifford group. A combination of RB with Monte Carlo sampling can be applied to still keep parts of the benefits of IRB [8].

That being said, in many practical architectures, the only non-Clifford gate is the T-gate, a $\pi/4$ z-axis rotation which can be done in software to high precision, so it is not crucial to calibrate it with optimal control. Also, as the two-qubit CNOT gate is a Clifford gate, one cannot claim that natively and without error correction Clifford gates are easier than non-Clifford.

3.5 Approximating time evolutions with the Magnus expansion

Control calculations involve solving the time-dependent Schrödinger equation. While this can be done analytically in, e.g., rotating wave situations or approximations, this can quickly become hard – even for a system as simple as a harmonically driven two-state-system this is a daunting task [18]. If we would like to proceed analytically with optimal control as far as possible, computing the final gate analytically is a key ingredient to which the Magnus expansion is an important ingredient. Numerically, techniques for coupled ordinary differential equations like Runge-Kutta can be used as well as split-operator techniques. For analytical calculations, one can use the Dyson series familiar from regular advanced quantum mechanics as systematic

perturbation theory. In many cases, it is however more effective to use the Magnus expansion, an asymptotic expansion that used the number of nested commutators as a small parameter. It is exact but usually truncated at low order. Our treatment mostly follows [64].

The problem at hand is to start from a Hamiltonian that has a (hopefully) large but solvable component and a perturbation $\hat{H} = \hat{H}_0(t) + \hat{V}(t)$. A clever choice of this division is key and there is no need for the former to be time-independent. We can transfer to the interaction picture with respect to \hat{H}_0 . The resulting transformed perturbation $\hat{V}^I(t)$ will then acquire additional time-dependence, often in the form of large oscillating terms. The objective is now to approximately calculate the time evolution

$$\hat{U}^I(t) = \mathbb{T} \exp \left(-\frac{i}{\hbar} \int_0^t d\tau \hat{V}^I(\tau) \right)$$

where \mathbb{T} is the usual time ordering operator. The Dyson expansion of this term starts as

$$\hat{U}^I(t) = 1 - \frac{i}{\hbar} \int_0^t d\tau \hat{V}^I(\tau) - \frac{1}{\hbar^2} \int_0^t d\tau \int_0^\tau d\tau' \hat{V}^I(\tau) \hat{V}^I(\tau') + \dots$$

which we can expect to converge quickly if the perturbation combined with oscillations are so small that the integration over (potentially) long times does not hinder convergence. If this is not the case, one could resort to self-energy techniques as they are known in quantum field theory. For these time-dependent systems, the Magnus expansion is a related route. It provides an expansion

$$\hat{U}^I(t) = e^{-i \sum_{n=0}^{\infty} \bar{H}_n(t)} \quad (25)$$

thus truncating this series happens in the exponent and maintains unitarity and is compatible with going to long times. Its lowest orders can be understood as follows: We start with the average Hamiltonian

$$\bar{H}_0(t) = \int_0^t d\tau \hat{V}^I(\tau)$$

i.e. the expression that collects the classical part and ignores all commutators. The next order contains one commutator

$$\bar{H}_1(t) = -\frac{i}{2} \int_0^t d\tau_1 d\tau_2 \left[\hat{V}^I(\tau_2), \hat{V}^I(\tau_1) \right]$$

but as it is in the exponent, it collects terms from all orders of the Dyson series (you can convince yourself by expanding the exponential in eq. (25)). The next order of the expansion is

$$\bar{H}_2(t) = -\frac{1}{6} \int_0^t d\tau_1 d\tau_2 d\tau_3 \left\{ \left[\hat{V}^I(\tau_3), \left[\hat{V}^I(\tau_2), \hat{V}^I(\tau_1) \right] \right] + \left[\hat{V}^I(\tau_1), \left[\hat{V}^I(\tau_2), \hat{V}^I(\tau_3) \right] \right] \right\}$$

i.e. it contains two nested commutators. We will only be able to appreciate this expansion when we apply it, but we can already see that the different orders will inherit different operator structures from the different commutators and that stacking on more integrals will create ever more demanding resonance conditions, so higher orders likely oscillate out. That notwithstanding, the Magnus expansion is asymptotic in nature: Its formal radius of convergence is zero hence adding higher orders does not always improve the accuracy.

3.6 Real-world limitations

When applying (quantum) optimal control to real-world systems, we have to contend with the fact that all parameters under our control have practical limitations: power, frequency, timing, etc. are all constrained by the capabilities of the equipment through which we apply said control. Moreover, any feedback scheme (such as Ad-HOC), must account for experimental noise, uncertainties in the experimental system (both gaps in system characterization, and "random walk"-like drifts of experimental parameters) and imperfections in both control and readout.

These issues above are complex and have to be dealt with simultaneously in real-world scenarios. There is no known textbook solution to these problems, and they are subject to ongoing research. We shall therefore limit ourselves to a very brief review of some of the approaches currently available:

Constraints on applicable controls: Two approaches can be taken: Either the space of possible controls can be defined such all points in the search space are valid, applicable, controls, or the optimization space is defined more liberally, and we penalize controls which fail to conform.

For the first approach, limiting the control subspace, a partial solution is to choose and fix some parameters, such as control field frequency, ahead of time. This is the solution suggested by the CRAB optimal control algorithm [13]. A more general approach is to use bounded functions, such as cosine or inverse tangent, to transform an unconstrained physical parameter to a constrained one. For example, the search parameter α may be unconstrained and $\mathcal{O}(1)$, and we transform it to a constrained field amplitude via $A := 500\text{MHz} \times \cos(\alpha)$, which is subsequently used in the system Hamiltonian.

Sometimes, the approaches above are insufficient as constraints are complex and include multiple parameters; or perhaps such substitutions are not a good fit to the optimal control problem. In such cases, we can impose a penalty term which will modify the functional for which we seek a minimum. For example, if we wish to impose a low-bandwidth solution on the control field $c(t)$, we may add a penalty term proportional to $\int_0^T |\partial_t c(t)|^2 dt$, which will be significant for highly oscillatory functions and zero for the DC component.

Robust controls: Experiments are often noisy environments, which noise appearing both on control fields and on the underlying system Hamiltonians. To provide a control scheme which provides consistently good performance, one must add the robustness requirement of the optimization requirements. This can be done using "ensemble optimization", where each optimization step averages over multiple manifestations of the dynamics, each with a different noise realization. The specific noise manifestations can be either fixed for the duration of the optimization or varied with each iteration step. The former approach is simpler to implement, but runs the risk of the optimization solving the problem only to the small subset of noises it encountered. The latter approach tends to result in more robust controls, but introduces a noisy goal function, which is harder to optimize reliably. In either case, ensemble optimization tends to be expensive in terms of computational resources. In some cases, it is possible to replace it with the a penalty term which is proportional to the absolute value of the gradient of the standard optimization goal with respect to the noisy variable (i.e. require that the control's performance will be weakly dependent on the noisy parameter). In all cases, robust controls often exhibit the "no free lunch" rule of control theory – robust controls often require more time, more bandwidth, or provide a worst average-case performance than their non-robust counterparts [30].

4 Examples

4.1 Optimal control of a qubit

Let's start with a really elementary analytical example: A single qubit with Hamiltonian $\hat{H}(t) = u(t)\hat{\sigma}_x$ looking at the fastest state transfer possible from $|0\rangle$ to $e^{i\phi}|1\rangle$. We can parameterize the state as $|\psi\rangle(t) = (x_0 + iy_0)|0\rangle + (x_1 + iy_1)|1\rangle$. The Schrödinger equation can be expressed in these real parameters as

$$\dot{x}_0 = uy_1 \quad \dot{y}_0 = -ux_1 \quad \dot{x}_1 = uy_0 \quad \dot{y}_1 = -ux_0$$

which are coupled in two sets of two that do not talk to the other components, already telling us that $\phi = \pm\pi/2$. Keep in mind, however, that u can be time-dependent. Now we clearly see that the speed of evolutions scales with the control amplitude u so our initial question was not even well-posed. We need to at least limit the amplitude of the control field. We make this dimensionless $|u| \leq u_{\max}$. The optimal solution exhausts that amplitude and, indeed, plugging in $u = u_{\max}$ we find

$$\ddot{x}_0 + u_{\max}^2 x_0 = 0$$

the harmonic oscillator equation of motion which leads to the desired solution $x_0 = 0$ after time $t_{\min} = \pi/2u_{\max}$. Solutions of this kind are called “bang” solutions. More generally, in strictly bilinear control problems like this one, the optimal solution jumps between its boundaries (which in the case of multiple controls can be quite intricate), then called “bang-bang”-control.

It is interesting to study the physical significance of this result. A real system in its laboratory frame always has an attached drift

$$\hat{H}_1(t) = \frac{E}{2}\hat{\sigma}_z + u(t)\hat{\sigma}_x$$

Now if $u_{\max} \gg |E|$ we can expect the previous solution to still hold approximately. If this condition is violated, the situation is different: The vectors $(\pm u_{\max}, y, z)^T$ define two non-collinear axes on the Bloch sphere and a given initial state can reach all final states that are on the circle around that axis including that state. In general, we will need up to three “bangs” to reach our goal. The limitation of u_{\max} may

4.2 Exploring the speed limit with high parameter counts

The quantum speed limit (QSL) is defined as the minimal time that is needed to evolve a system from a given state ρ_0 to another state $\rho(t)$ with a specific fidelity $\Phi(\rho_0, \rho(t))$ [19]. This is relevant e.g. for qubit gate implementations, because it limits the minimal gate time (for unrestricted controls). When the control bandwidth is restricted, then the dimension of the set of reachable states $D_{\mathcal{W}}$ and the available bandwidth $\Delta\Omega$ give a lower bound for the evolution time [37]:

$$T \geq \frac{D_{\mathcal{W}}}{\Delta\Omega}$$

This is a continuous version of the Solovay-Kitaev theorem.

The set of reachable states consists of all states that can be written as

$$|\psi(t)\rangle = U(t_0, t)|\psi_0\rangle \quad (26)$$

where $U(t_0, t)$ is the propagation operator of the system. A system is called completely controllable if one can choose the control parameters in such a way that the propagation operator is equal to any specific operator [57].

A method to explore the QSL for a gate is the following [60]: For different given gate times one optimizes the gate and plots the fidelity Φ_{goal} or the error $g(T) = 1 - \Phi_{\text{goal}}$ (see equation (21)) of the optimized gates against the gate times. If a QSL exists, there will be minimal time for which the error is small. For shorter gate times the error is significantly larger. This time is the QSL.

The result depends on the chosen optimization method, concretely we show an example:

In fig. 6 and fig. 7 the error g is plotted against gate duration for two different parameterizations. The system is a CR-gate implementation of a CNOT gate [31].

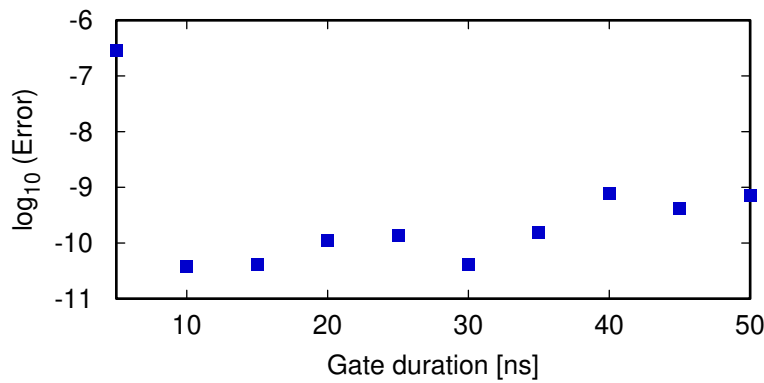


Figure 6: Gate error as a function of gate time. The optimization was done using GRAPE with a PWC parameterization with 500 pieces. The QSL is around 10ns.

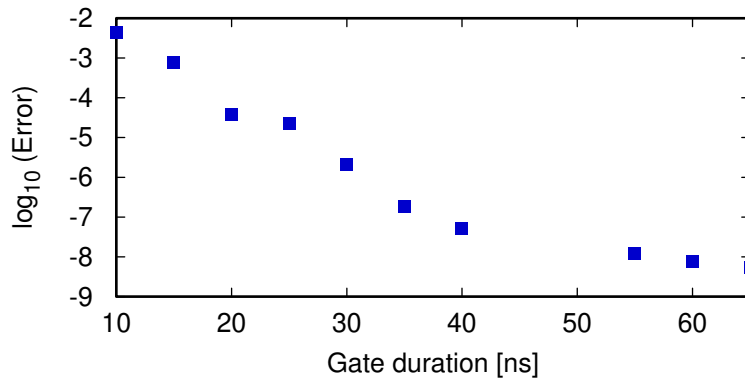


Figure 7: Gate error as a function of gate time. The optimization was done using GOAT with a Fourier decomposition into 167 pieces. The QSL is around 40ns.

In fig. 6 the QSL is shown for a piecewise constant (PWC) parameterization with 500 pieces and unconstrained controls. One can see that there is a jump around 10ns which indicates that

this is the QSL in this case. Fig. 7 shows the same, but with a Fourier decomposition into 167 components. The QSL is here around 40ns and is reached more slowly.

The difference is related to optimally have the controls interact with redirecting the drift. A key step to a theory of this phenomenon has been undertaken in [37].

4.3 Open systems

In these notes we have mostly concentrated on the optimal control for closed quantum systems. One can ask related questions for open quantum systems as well. A treatment of this situation would go way beyond the scope of these lecture notes. Here, the space of potentially reachable states / of reachable time evolutions is much larger than in the unitary case. The theory of controllability and reachability is thus more involved, it is for example not at all clear, if the impact of decoherence can be reduced to zero, i.e., if the subset of unitary time evolutions is reachable. We would thus like to describe a pragmatic approach and refer the reader to the literature. For a Lindblad equation, it can be shown that the control fields cannot cancel dissipation effect and the system is not completely controllable. This is still an open question in the non-Markovian regime.

As a first rule of thumb, there are situations when the decoherence experienced by the quantum subsystem has no or very little structure – e.g. in the case of uniform decoherence leading to a fully depolarizing channel and, at least for the synthesis of gates, for most Markovian decoherence models. These do not give an open system optimal control algorithm any space to actually exploit the structure of the decoherence to perform an optimization, rather, we can expect that the fastest solution of the closed system also is close to an optimal solution for the open system. Thus, running a closed-system version of optimal control and benchmarking it in a realistic open system is a good initial approach.

If one suspects that the decoherence mechanism contains exploitable structure, or if one tries to accomplish a task that actively uses decoherence – such as tasks changing the entropy of the state, e.g., cooling, it is possible to generalize the aforementioned methods of optimal control. More specifically, e.g., in OpenGRAPE, one simply replaces the Schrödinger equation as the dynamical constraint by a suitable description of open systems dynamics, such as a master equation. One caveat lies in the need for backwards-in-time propagation: Open system dynamics is asymptotically irreversible, which can make back-propagation unstable. Practically, this can be handled by either focusing on decoherence rates that are not too large or by suitable initial guesses.

As a well-defined example, let us consider a single qubits perturbed by a two-level fluctuator, i.e., a second two-state system that is coupled to a heat bath. This is a common situation in superconducting qubits [54].

We specifically model a qubit coupled to a single TLF by $H = H_S + H_I + H_B$. H_S consists of the qubit and the coupled two-state system, i.e.

$$H_S = E_1(t)\sigma_z + \Delta\sigma_x + E_2\tau_z + \Lambda\sigma_z\tau_z$$

where σ_i and τ_i are the usual Pauli matrices operating in qubit and fluctuator Hilbert space respectively. $E_1(t)$ is time-dependent and serves as an external control. The source of decoherence is the coupling of the fluctuator to the heat bath, which leads to incoherent transitions

between the fluctuator eigenstates, $H_I = \sum_i \lambda_i (\tau^+ b_i + \tau^- b_i^\dagger)$, $H_B = \sum_i \hbar \omega_i b_i^\dagger b_i$. We introduce an Ohmic bath spectrum $J(\omega) = \sum_i \lambda_i^2 \delta(\omega - \omega_i) = \kappa \omega \Theta(\omega - \omega_c)$ containing the couplings λ_i , the dimensionless damping κ , and a high-frequency cutoff ω_c (which we assume to be the largest frequency in the system). Now depending on the bath damping constant κ the fluctuator can flip fast or slow – and in the limit of slow flipping, the qubit sees noise with strong temporal correlation leading to highly non-Markovian qubit dynamics.

To formally treat this system, we can on the other hand still set up a Markovian master equation for the augmented system of qubit *and* fluctuator and only after its solution trace over the fluctuator to get the effective density matrix of the qubit alone. We formulate the control approach by rewriting the master equation as $\dot{\rho}(t) = -(i\mathcal{H}(E_1(t)) + \Gamma(E_1(t)))\rho(t)$ with the Hamiltonian commutator superoperator $\mathcal{H}(E_1(t))(\cdot) = [H(E_1(t)), \cdot]$ and the relaxation superoperator Γ , both time-dependent via the control $E_1(t)$. The formal solution to the master equation is a linear quantum map operating on a physical initial state according to $\rho(t) = F(t)\rho(0)$. Thus F itself follows the operator equation of motion

$$\dot{F} = -(i\mathcal{H} + \Gamma) F \quad (27)$$

with initial condition $F(0) = \mathbb{I}$, as in ref. [58].

Here, multiplication of quantum maps denotes their concatenation. The task is to find control amplitudes $E_1(t)$ with $t \in [0, t_g]$, t_g being a fixed final time, such that the difference $\delta F = F_U - F(t_g)$ between dissipative time evolution $F(t_g)$ obeying eqn. (27) and a target unitary map F_U is minimized with respect to the Euclidean distance $\|\delta F\|_2^2 \equiv \text{tr} \{ \delta F^\dagger \delta F \}$. Clearly, this is the case, when the trace fidelity

$$\phi = \text{Re tr} \left\{ F_U^\dagger F(t_g) \right\} \quad (28)$$

is maximal. Note, that in an open system, one cannot expect to achieve zero distance to a unitary evolution F_U [58]. The goal is to come as close as possible. On this setting, we find optimal pulses by gradient search.

It is interesting to investigate the resulting pulses and performance limits. We see in figure ... that optimal control pulses allow to reach great gate performance after overcoming a quantum speed limit. Remarkably, the dependence on gate duration is non-monotonic at least in the regime of low κ when the two settings of the TLS can be resolved. At some magic times, the frequency split from the TLS naturally refocuses, constraining the optimization much less than at other times.

More remarkable, the maximally attainable fidelity also has a non-monotonic dependence on κ . At hindsight, this can be understood as follows: At low κ there is no randomness of the system, it is fully reversible. The optimal control algorithm just has to deal with the fact that the setting of the TLS is unknown, which it perfectly accomplishes. On the other hand, at high κ , the phenomenon of *motional narrowing* occurs: Fast motion of the impurity broadens its spectrum thus reducing its spectral weight at low frequencies.

4.4 DRAG and its derivatives

In general a quantum system will contain additional states outside of a specific subspace we want to operate in. If our control couples also to transitions out of the subspace we will leak

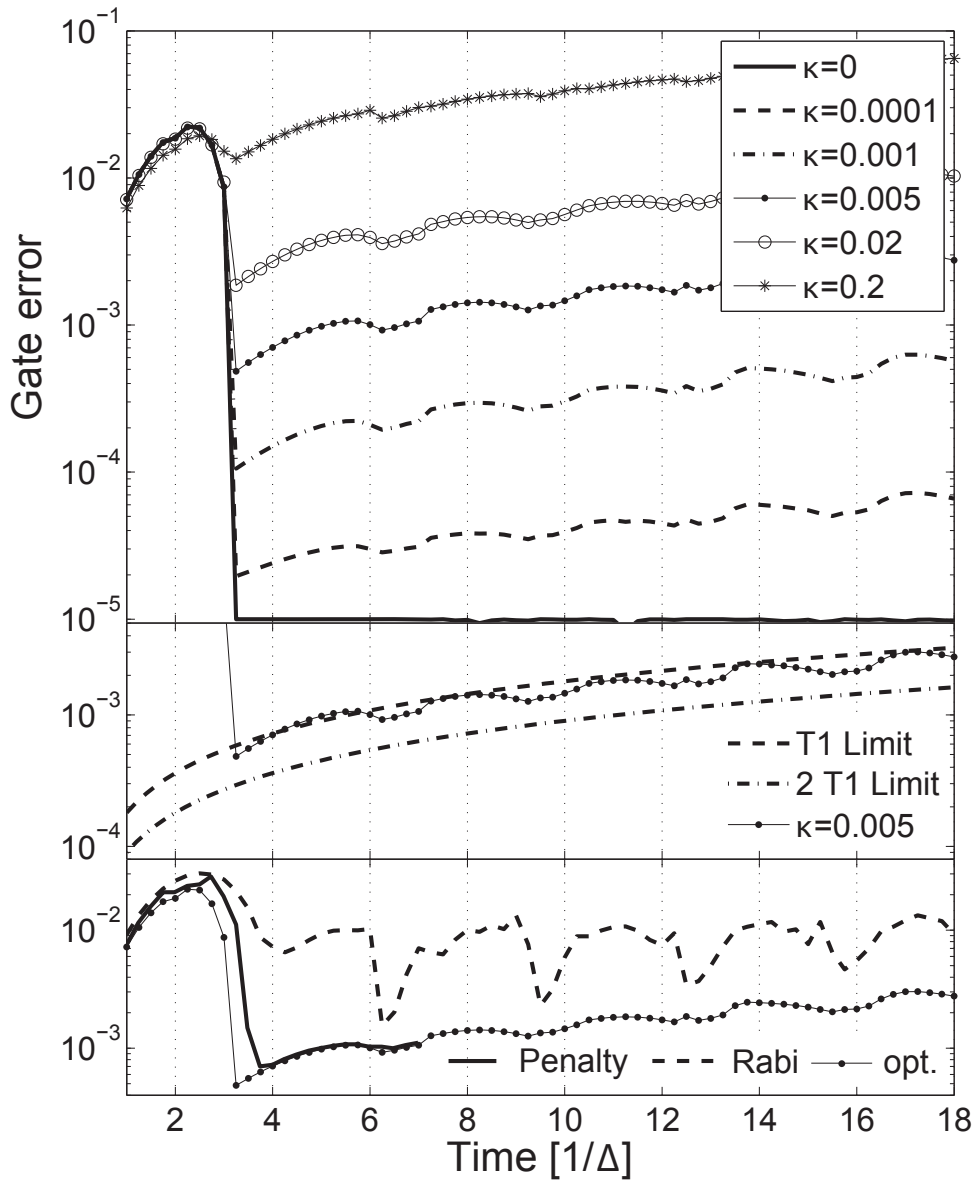


Figure 8: Top: Gate error versus pulse time t_g for optimal Z-gate pulses in the presence of a non-Markovian environment with dissipation strength κ . A periodic sequence of minima at around $t_n = n\pi/\Delta$, where $n \geq 1$, is obtained. Middle: The gate error of optimized pulses approaches a limit set by T_1 and $2T_1$, as shown with $\kappa = 0.005$. Bottom: Optimized pulses reduce the error rate by approximately one order of magnitude compared to Rabi pulses for $\kappa = 0.005$. Pulses starting from zero bias and with realistic rise times (penalty) require only a small additional gate time. In all figures the system parameters are $E_2 = 0.1\Delta$, $\Lambda = 0.1\Delta$ and $T = 0.2\Delta$.

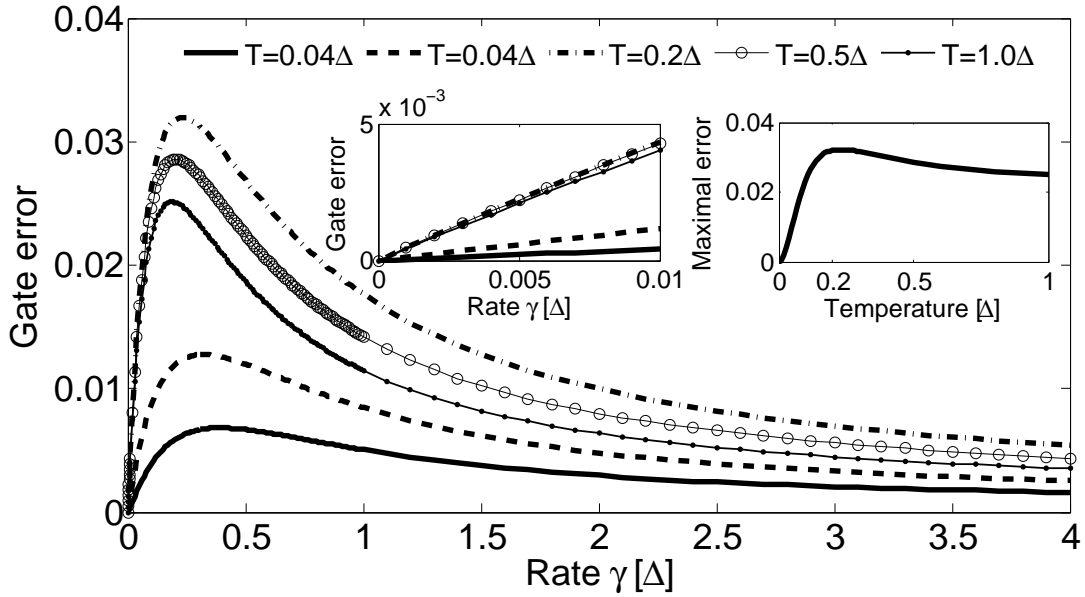


Figure 9: Gate error versus TLF rate γ for various temperatures for an optimized pulse with $t_g = 5.0/\Delta$. The left inset is a magnification of the low- γ part of the main plot and reveals the linear behaviour. The right inset shows the maximum of the curves of the main plot versus temperature. ($E_2 = 0.1\Delta$ and $\Lambda = 0.1\Delta$)

population and degrade the performance of our operation. The Derivative Removal with Adiabatic Gate (DRAG) method provides a framework to identify these leakages and to modify the control signals to counteract them.

We will review the basic idea along the procedure shown in [45]. Consider a 3-level-system that is controlled by a signal $u(t) = u_x(t) \cos(\omega_d t) + u_y(t) \sin(\omega_d t)$. The first two levels make up the computational subspace $|0\rangle, |1\rangle$ with transition frequency ω_1 that we want to operate in and $|2\rangle$ accounts for the leakage. It is modeled by the Hamiltonian

$$H/\hbar = \omega_1 |1\rangle \langle 1| + (2\omega_1 + \Delta) |2\rangle \langle 2| + u(t)\hat{\sigma}_{0,1}^x + \lambda u(t)\hat{\sigma}_{1,2}^x \quad (29)$$

where the Pauli operators are $\hat{\sigma}_{j,k}^x = |k\rangle \langle j| + |j\rangle \langle k|$ and λ describes the coupling of the drive to the 1-2 transition. We expressed the second transition frequency by the anharmonicity $\Delta = \omega_2 - 2\omega_1$.

Let's say we want to implement a simple Rabi pulse by choosing $u_x(t) = \Omega(t)$ and $u_y(t) = 0$. This gives rise to unwanted leakage out of the computational subspace with the term $\lambda\Omega(t)\hat{\sigma}_{1,2}^x$. The DRAG idea shows how we can counteract this leakage by choosing $u_y(t)$ appropriately.

We first express the Hamiltonian in the rotating frame with $R = \exp(i\omega_d |1\rangle \langle 1| + 2i\omega_d |1\rangle \langle 1|)$ following the rule $H^R = RHR^\dagger + i\hbar\dot{R}R^\dagger$ which gives

$$H^R/\hbar = \delta_1 |1\rangle \langle 1| + \delta_2 |2\rangle \langle 2| + \sum_{\alpha=x,y} \frac{u_\alpha}{2}(t)\hat{\sigma}_{0,1}^\alpha + \lambda \frac{u_\alpha}{2}(t)\hat{\sigma}_{1,2}^\alpha,$$

using the detunings $\delta_1 = \omega_1 - \omega_d$ and $\delta_2 = \Delta + 2\delta_1$ between the drive and transition frequencies.

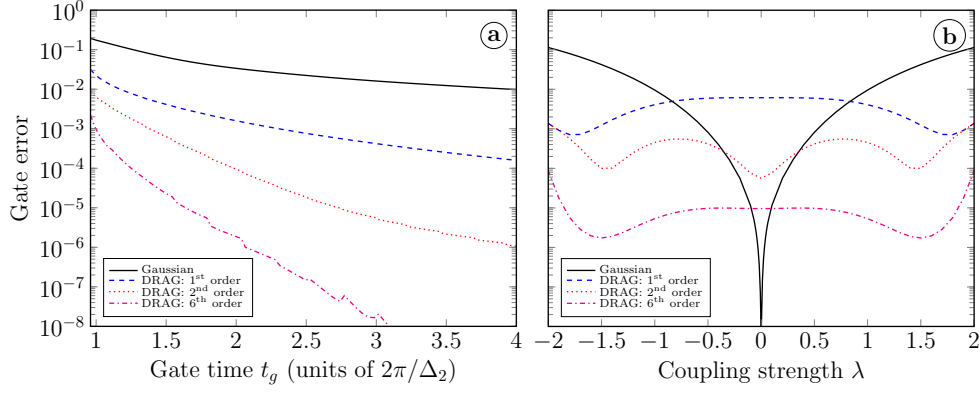


Figure 10: (a): Performance of non-optimized DRAG variants as a function of gate time, derived from an iterative Schrieffer-Wolff expansion to higher orders. Target : $\hat{\sigma}_x$ rotation of a single qubit described by the lowest three levels of Hamiltonian (29). – (b): Performance of the DRAG pulses used in (a) for a fixed gate time $t_g = 4\pi/\Delta_2$ as a function of coupling strength λ to the leakage level.

Applying an adiabatic transformation $V(t)$ by calculating $H^V = VHV^\dagger + i\hbar\dot{V}V^\dagger$ allows us to look at the system in a frame where the leakage and the y -component necessary to counteract it are visible. We take

$$V(t) = \exp \left[-i \frac{u_x(t)}{2\Delta} (\hat{\sigma}_{0,1}^y + \lambda \hat{\sigma}_{1,2}^y) \right],$$

a transformation that depends on our intended signal u_x , and apply it to first order in u_x/Δ to find

$$\begin{aligned} H^V/\hbar = & \left(\delta_1 - \frac{(\lambda^2 - 4)u_x^2}{4\Delta} \right) |1\rangle\langle 1| + \left(\delta_2 + \frac{(\lambda^2 + 2)u_x^2}{4\Delta} \right) |2\rangle\langle 2| \\ & + \frac{u_x}{2} \hat{\sigma}_{0,1}^x + \lambda \frac{u_x^2}{8\Delta} \hat{\sigma}_{0,2}^x + \left[\frac{u_y}{2} + \frac{\dot{u}_x}{2\Delta} \right] (\hat{\sigma}_{0,1}^y + \lambda \hat{\sigma}_{1,2}^y) \end{aligned}$$

From this expression we can see that our intended drive is unchanged $u_x/2\hat{\sigma}_{0,1}^x$ but if we also choose $u_y = -\dot{u}_x/\Delta$ we cancel the last term that is responsible for driving out of the computational subspace $\propto \lambda \hat{\sigma}_{1,2}^y$. The transformation also suggest detuning the drive by $\delta_1 = (\lambda^2 - 4)u_x^2/4\Delta$ to avoid stark shifting of the 0-1 transition. This example illustrates the main working principle of DRAG which can be generalized to account for more than just leakage to a third level. By modifying $V(t)$, for example adding terms $\propto \hat{\sigma}_{0,2}^y$, or iteratively performing transformations $V_j(t)$ the inertial terms, the inertial terms $i\hbar\dot{V}_jV_j^\dagger$ generate more conditions on the control signals and its derivatives.

The performance of solutions to different orders, obtained via iterative transformations, is depicted in Fig.10a as a function of pulse length, and in Fig.10b as a function of coupling strength λ for a fixed gate time $t_g = 4\pi/\Delta_2$. Higher order solutions are taken from [46]. Note also that when the $|0\rangle \leftrightarrow |2\rangle$ transition is controlled via an additional corresponding frequency component, exact solutions to the three-level system exist (cf. chapter 8 in [43]).

Turning to the experimental implementation [11, 38] of DRAG pulses: In practice, actual system parameters differ somewhat from those assumed in theory due to characterization gaps, system drift, or unknown transfer functions affecting the input field shapes [44]. As a simplifi-

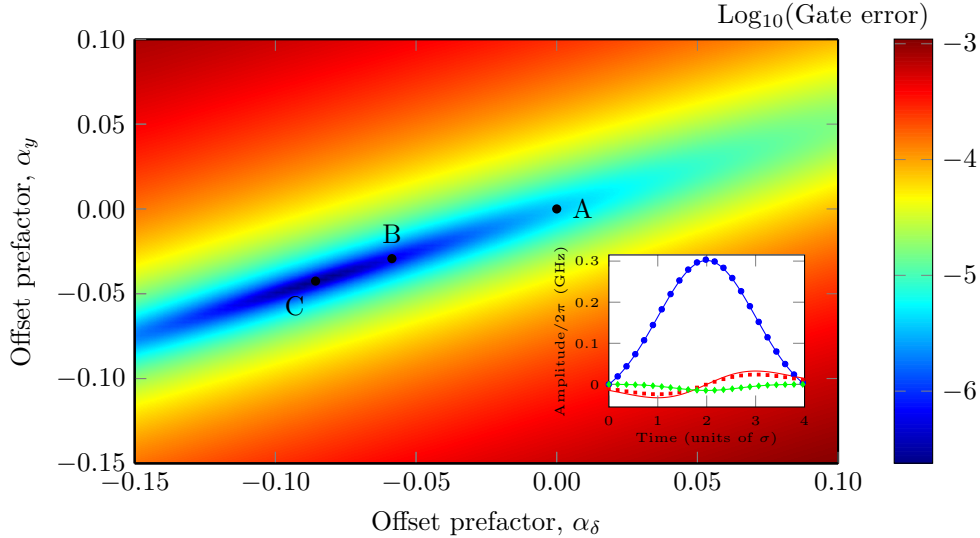


Figure 11: A slice of the 3D calibration landscape for DRAG solution up to the first order in the small parameter to the qubit σ_x -gate leakage problem. Point A and B denote [45]’s and [17]’s first-order solutions, respectively. Point C is the optimum for this control function subspace (here $\alpha_x = -0.0069$), with infidelity of $10^{-6.63}$. A successful calibration process will typically start at a known DRAG solution, i.e. points A or B, and conclude in point C. The inset illustrates the associated pulse shapes: markers represent the unoptimized shapes (u_x : \bullet , u_y : \blacksquare , δ : \blacklozenge) whereas solid lines depict the corresponding optimal solution (C).

cation, we assume the low order terms in DRAG are easier to implement as their shape will be mostly maintained on entry into the dilution fridge. Even so, many different low-order variants of DRAG have been found in the literature for third-level leakage [17, 38, 45, 46]. This reduced functional form can further be optimized theoretically [63] and/or through a closed-loop process experimentally [14, 28] to account for the effect of higher order terms and experimental uncertainties (preferably using more advanced gradient-free algorithms such as CMA-ES [25]). A systematic experimental study of the tune-up of the prefactors in front of the functional forms for the control operators was performed in [10]. In writing up these optimizations and adapting them, the Magnus expansion, see chapter 3.5 is typically used.

For instance, let us denote the Gaussian pulse implementing a $\hat{\sigma}_x$ gate for the qubit by $G(t)$. Then the first order solutions described in [17, 45, 46] are parameterized by the limited functional basis $u_x \propto G$, $u_y \propto \partial_t G$ and $\delta \propto G^2$, which mimics the limited shaping control that can exist in experiment. None of the reported solutions are optimal within this functional basis: For typical example parameters, infidelities may be further reduced from $10^{-5.28}$ to $10^{-6.63}$ by slightly adjusting the prefactors of the control fields. For example, [45]’s first order DRAG solution may be transformed according to $u_x \rightarrow (1 + \alpha_x)u_x$ and similarly for u_y and δ , and then the constants α_x , α_y and α_δ are optimized. A discussion for why optimization within a severely restricted functional subspace may often be sufficient is given in [7] and follow-up publications. A schematic of the optimization task involved in the calibration, as well as the shape of the associated controls, is shown in Fig.11.

5 Summary and outlook

Optimal control is a mature discipline of theoretical physics and related fields. In experimentation, it has remarkable success in situations in which physical systems are well characterized. Reaching out to engineered systems requires a close integration with characterization and benchmarking.

Experimentalists and users of quantum control should have taken home an introduction of concepts, jargon, and results of the field. Theorists should feel motivated to embrace these challenges and to fashion their results into tools that can be used efficiently and scalably so quantum control and quantum technology applications can mutually benefit from their potential.

Acknowledgements

We acknowledge collaboration with the optimal control group at Saarland University (and its previous locations), including Daniel Egger, Likun Hu, Kevin Pack, Federico Roy, Ioana Serban, and Lukas Theis as well as continuous collaboration with Tommaso Calarco, Steffen Glaser, Christiane Koch, Simone Montangero, and Thomas Schulte-Herbrüggen. Some of this work is sponsored by the Intelligence Advanced Research Projects Activity (IARPA) through the LogiQ Grant No. W911NF-16-1-0114, by the European Union under OpenSuperQ and the ITN Qusco.

References

- [1] ACÍN, A., BLOCH, I., BUHRMAN, H., CALARCO, T., EICHLER, C., EISERT, J., ESTEVE, D., GISIN, N., GLASER, S. J., JELEZKO, F., KUHR, S., LEWENSTEIN, M., RIEDEL, M. F., SCHMIDT, P. O., THEW, R., WALLRAFF, A., WALMSLEY, I., AND WILHELM, F. K. The quantum technologies roadmap: a European community view. *New J. Phys.* 20, 8 (aug 2018), 080201.
- [2] AIZU, K. Parameter differentiation of quantum-mechanical linear operators. *Journal of Mathematical Physics* 4, 6 (1963), 762–775.
- [3] ANDRESEN, B., HOFFMANN, K. H., NULTON, J., TSIRLIN, A., AND SALAMON, P. Optimal control of the parametric oscillator. *European journal of physics* 32, 3 (2011), 827.
- [4] ANGARONI, F., GRAUDENZI, A., ROSSIGNOLO, M., MASPERO, D., CALARCO, T., PIAZZA, R., MONTANGERO, S., AND ANTONIOTTI, M. Personalized therapy design for liquid tumors via optimal control theory. *bioRxiv* (2019), 662858.
- [5] BINDER, J. M., STARK, A., TOMEK, N., SCHEUER, J., FRANK, F., JAHNKE, K. D., MÜLLER, C., SCHMITT, S., METSCH, M. H., UNDEN, T., ET AL. Qudi: A modular python suite for experiment control and data processing. *SoftwareX* 6 (2017), 85–90.

- [6] BRYSON, A. E., AND HO, Y.-C. Applied optimal control, revised printing. *Hemisphere, New York* (1975).
- [7] CANEVA, T., CALARCO, T., AND MONTANGERO, S. Chopped random-basis quantum optimization. *Phys. Rev. A* *84* (Aug 2011), 022326.
- [8] CHASSEUR, T., REICH, D. M., KOCH, C. P., AND WILHELM, F. K. Hybrid benchmarking of arbitrary quantum gates. *PHYSICAL REVIEW A* *95*, 6 (JUN 27 2017).
- [9] CHASSEUR, T., AND WILHELM, F. K. Complete randomized benchmarking protocol accounting for leakage errors. *Phys. Rev. A* *92* (Oct 2015), 042333.
- [10] CHEN, Z., KELLY, J., QUINTANA, C., BARENDS, R., CAMPBELL, B., CHEN, Y., CHIARO, B., DUNSWORTH, A., FOWLER, A., LUCERO, E., JEFFREY, E., MEGRANT, A., MUTUS, J., NEELEY, M., NEILL, C., O'MALLEY, P., ROUSHAN, P., SANK, D., VAINSENER, A., WENNER, J., WHITE, T., KOROTKOV, A., AND MARTINIS, J. M. Measuring and suppressing quantum state leakage in a superconducting qubit. *Phys. Rev. Lett.* *116* (Jan 2016), 020501.
- [11] CHOW, J. M., DICARLO, L., GAMBETTA, J. M., MOTZOI, F., FRUNZIO, L., GIRVIN, S. M., AND SCHOELKOPF, R. J. Optimized driving of superconducting artificial atoms for improved single-qubit gates. *Phys. Rev. A* *82* (Oct 2010), 040305.
- [12] DANKERT, C., CLEVE, R., EMERSON, J., AND LIVINE, E. Exact and approximate unitary 2-designs and their application to fidelity estimation. *Phys. Rev. A* *80* (Jul 2009), 012304.
- [13] DORIA, P., CALARCO, T., AND MONTANGERO, S. Optimal control technique for many-body quantum dynamics. *Phys. Rev. Lett.* *106* (May 2011), 190501.
- [14] EGGER, D. J., AND WILHELM, F. K. Adaptive hybrid optimal quantum control for imprecisely characterized systems. *Physical review letters* *112*, 24 (2014), 240503.
- [15] EMERSON, J., ALICKI, R., AND ŻYCZKOWSKI, K. Scalable noise estimation with random unitary operators. *Journal of Optics B: Quantum and Semiclassical Optics* *7*, 10 (sep 2005), S347–S352.
- [16] FERRIE, C., AND MOUSSA, O. Robust and efficient in situ quantum control. *Phys. Rev. A* *91* (May 2015), 052306.
- [17] GAMBETTA, M., J., MOTZOI, F., MERKEL, T., S., WILHELM, AND K., F. Analytic control methods for high-fidelity unitary operations in a weakly nonlinear oscillator. *Phys. Rev. A* *83* (2011), 012308.
- [18] GANGOPADHYAY, A., DZERO, M., AND GALITSKI, V. Exact solution for quantum dynamics of a periodically driven two-level system. *Phys. Rev. B* *82* (Jul 2010), 024303.
- [19] GIOVANNETTI, V., LLOYD, S., AND MACCONE, L. Quantum limits to dynamical evolution. *Phys. Rev. A* *67* (May 2003), 052109.

- [20] GLASER, S. J., BOSCAIN, U., CALARCO, T., KOCH, C. P., KÖCKENBERGER, W., KOSLOFF, R., KUPROV, I., LUY, B., SCHIRMER, S., SCHULTE-HERBRÜGGEN, T., SUGNY, D., AND WILHELM, F. K. Training Schrödinger’s cat: quantum optimal control. *Eur. Phys. J. D* 69, 12 (dec 2015).
- [21] GOERZ, M. H., BASILEWITSCH, D., GAGO-ENCINAS, F., KRAUSS, M. G., HORN, K. P., REICH, D. M., AND KOCH, C. P. Krotov: A Python implementation of Krotov’s method for quantum optimal control. *SciPost Phys.* 7 (2019), 80.
- [22] GROSS, D., LIU, Y.-K., FLAMMIA, S. T., BECKER, S., AND EISERT, J. Quantum state tomography via compressed sensing. *Phys. Rev. Lett.* 105 (Oct 2010), 150401.
- [23] HALL, B. C. An elementary introduction to groups and representations. arXiv:math-ph/0005032.
- [24] HALL, B. C. *Lie Groups, Lie Algebras, and Representations*, vol. 222 of *Graduate Texts in Mathematics*. Springer, New York, 2003.
- [25] HANSEN, N., MÜLLER, S. D., AND KOUMOUTSAKOS, P. Reducing the Time Complexity of the Derandomized Evolution Strategy with Covariance Matrix Adaptation (CMA-ES). *Evol. Comput.* 11, 1 (mar 2003), 1–18.
- [26] HU, L. Optimal control with an arbitrary performance index. Honors Thesis, University of Waterloo, 2008.
- [27] JUDSON, R. S., AND RABITZ, H. Teaching lasers to control molecules. *Phys. Rev. Lett.* 68 (1992), 1500–1503.
- [28] KELLY, J., BARENDTS, R., CAMPBELL, B., CHEN, Y., CHEN, Z., CHIARO, B., DUNSWORTH, A., FOWLER, A. G., HOI, I.-C., JEFFREY, E., MEGRANT, A., MUTUS, J., NEILL, C., O’MALLEY, P. J. J., QUINTANA, C., ROUSHAN, P., SANK, D., VAINSENER, A., WENNER, J., WHITE, T. C., CLELAND, A. N., AND MARTINIS, J. M. Optimal quantum control using randomized benchmarking. *Phys. Rev. Lett.* 112 (Jun 2014), 240504.
- [29] KHANEJA, N., REISS, T., KEHLET, C., SCHULTE-HERBRÜGGEN, T., AND GLASER, S. J. Optimal control of coupled spin dynamics: design of nmr pulse sequences by gradient ascent algorithms. *Journal of Magnetic Resonance* 172, 2 (2005), 296 – 305.
- [30] KHANI, B., MERKEL, S. T., MOTZOI, F., GAMBETTA, J. M., AND WILHELM, F. K. High-fidelity quantum gates in the presence of dispersion. *Phys. Rev. A* 85 (Feb 2012), 022306.
- [31] KIRCHHOFF, S., KESSLER, T., LIEBERMANN, P. J., ASSÉMAT, E., MACHNES, S., MOTZOI, F., AND WILHELM, F. K. Optimized cross-resonance gate for coupled transmon systems. *Phys. Rev. A* 97 (Apr 2018), 042348.
- [32] KNILL, E., LEIBFRIED, D., REICHEL, R., BRITTON, J., BLAKESTAD, R. B., JOST, J. D., LANGER, C., OZERI, R., SEIDELIN, S., AND WINELAND, D. J. Randomized benchmarking of quantum gates. *Phys. Rev. A* 77 (Jan 2008), 012307.

- [33] KOSLOFF, R., RICE, S., GASPARD, P., TERSIGNI, S., AND TANNOR, D. Wavepacket dancing: Achieving chemical selectivity by shaping light pulses. *Chem. Phys.* 139 (1989), 201.
- [34] KROTOV, V., AND FELDMAN, I. Iteration method of solving the problems of optimal control. *Eng. Cybern* 21 (1983), 123.
- [35] LEVANTE, T., BREMI, T., AND ERNST, R. Pulse-sequence optimization with analytical derivatives. application to deuterium decoupling in oriented phases. *Journal of Magnetic Resonance, Series A* 121, 2 (1996), 167–177.
- [36] LIEBERMANN, P. J., AND WILHELM, F. K. Optimal Qubit Control Using Single-Flux Quantum Pulses. *PHYSICAL REVIEW APPLIED* 6, 2 (AUG 29 2016).
- [37] LLOYD, S., AND MONTANGERO, S. Information theoretical analysis of quantum optimal control. *Phys. Rev. Lett.* 113 (Jul 2014), 010502.
- [38] LUCERO, E., KELLY, J., BIALCZAK, R. C., LENANDER, M., MARIANTONI, M., NEELEY, M., O’CONNELL, A. D., SANK, D., WANG, H., WEIDES, M., WENNER, J., YAMAMOTO, T., CLELAND, A. N., AND MARTINIS, J. M. Reduced phase error through optimized control of a superconducting qubit. *Phys. Rev. A* 82 (Oct 2010), 042339.
- [39] M. A. NIELSEN, I. L. C. *Quantum Computation and Quantum Information*. Cambridge University Press, 2010.
- [40] MACHNES, S., ASSÉMAT, E., TANNOR, D., AND WILHELM, F. K. Tunable, flexible, and efficient optimization of control pulses for practical qubits. *Phys. Rev. Lett.* 120 (Apr 2018), 150401.
- [41] MACHNES, S., SANDER, U., GLASER, S. J., DE FOUQUIÈRES, P., GRUSLYS, A., SCHIRMER, S., AND SCHULTE-HERBRÜGGEN, T. Comparing, optimizing, and benchmarking quantum-control algorithms in a unifying programming framework. *Phys. Rev. A* 84 (Aug 2011), 022305.
- [42] MAGESAN, E., GAMBETTA, J. M., JOHNSON, B. R., RYAN, C. A., CHOW, J. M., MERKEL, S. T., DA SILVA, M. P., KEEFE, G. A., ROTHWELL, M. B., OHKI, T. A., KETCHEN, M. B., AND STEFFEN, M. Efficient measurement of quantum gate error by interleaved randomized benchmarking. *Phys. Rev. Lett.* 109 (Aug 2012), 080505.
- [43] MOTZOI, F. *Controlling Quantum Information Devices*. PhD thesis, U. Waterloo, 2012.
- [44] MOTZOI, F., GAMBETTA, J. M., MERKEL, S. T., AND WILHELM, F. K. Optimal control methods for rapidly time-varying Hamiltonians. *Phys. Rev. A* 84 (2011), 022307.
- [45] MOTZOI, F., GAMBETTA, J. M., REBENTROST, P., AND WILHELM, F. K. Simple Pulses for Elimination of Leakage in Weakly Nonlinear Qubits. *Phys. Rev. Lett.* 103 (2009), 110501.
- [46] MOTZOI, F., AND WILHELM, F. K. Improving frequency selection of driven pulses using derivative-based transition suppression. *Phys. Rev. A* 88 (2013), 062318.

- [47] NISKANEN, A., VARTIAINEN, J., AND SALOMAA, M. Optimal multiqubit operations for josephson charge qubits. *Phys. Rev. Lett.* 90 (2003), 197901.
- [48] NOCEDAL, J. Updating quasi-newton matrices with limited storage. *Mathematics of Computation* 35, 151 (sep 1980), 773–773.
- [49] PALAO, J. P., AND KOSLOFF, R. Quantum computing by an optimal control algorithm for unitary transformations. *Phys. Rev. Lett.* 89 (Oct 2002), 188301.
- [50] PARIS, M., AND REHACEK, J. *Quantum State Estimation*. Springer, Berlin, 2004.
- [51] PEIRCE, A. P., MOHAMMED, DAHLEH, A., AND RABITZ, H. Optimal control of quantum-mechanical systems: Existence, numerical approximation, and applications. *Phys. Rev. A* 37 (1988), 4950.
- [52] RABITZ, H. A., HSIEH, M. M., AND ROSENTHAL, C. M. Quantum optimally controlled transition landscapes. *Science* 303 (2004), 1998–2001.
- [53] RACH, N., MÜLLER, M. M., CALARCO, T., AND MONTANGERO, S. Dressing the chopped-random-basis optimization: A bandwidth-limited access to the trap-free landscape. *Phys. Rev. A* 92 (Dec 2015), 062343.
- [54] REBENTROST, P., SERBAN, I., SCHULTE-HERBRÜGGEN, T., AND WILHELM, F. Optimal control of a qubit coupled to a two-level fluctuator. [quant-ph/0612165](https://arxiv.org/abs/quant-ph/0612165).
- [55] REICH, D. M., NDONG, M., AND KOCH, C. P. Monotonically convergent optimization in quantum control using krotov’s method. *The Journal of Chemical Physics* 136, 10 (2012), 104103.
- [56] SANDERS, Y. R., WALLMAN, J. J., AND SANDERS, B. C. Bounding quantum gate error rate based on reported average fidelity. *New Journal of Physics* 18, 1 (2016), 012002.
- [57] SCHIRMER, S. G., SOLOMON, A. I., AND LEAHY, J. V. Degrees of controllability for quantum systems and application to atomic systems. *Journal of Physics A: Mathematical and General* 35, 18 (apr 2002), 4125–4141.
- [58] SCHULTE-HERBRÜGGEN, T., SPÖRL, A., KHANEJA, N., AND GLASER, S. J. Optimal control for generating quantum gates in open dissipative systems. *Journal of Physics B: Atomic, Molecular and Optical Physics* 44, 15 (jul 2011), 154013.
- [59] SILVI, P., RICO, E., CALARCO, T., AND MONTANGERO, S. Lattice gauge tensor networks. *New Journal of Physics* 16, 10 (2014), 103015.
- [60] SØRENSEN, J. J. W., PEDERSEN, M. K., MUNCH, M., HAIKKA, P., JENSEN, J. H., PLANKE, T., ANDREASEN, M. G., GAJDACZ, M., MØLMER, K., LIEBEROTH, A., ET AL. Exploring the quantum speed limit with computer games. *Nature* 532, 7598 (2016), 210.
- [61] SØRENSEN, J. J. W. H., ARANBURU, M. O., HEINZEL, T., AND SHERSON, J. F. Quantum optimal control in a chopped basis: Applications in control of bose-einstein condensates. *Phys. Rev. A* 98 (Aug 2018), 022119.

- [62] TESCH, C. M., KURTZ, L., AND DE VIVIE-RIEDLE, R. Applying optimal control theory for elements of quantum computation in molecular systems. *Chemical Physics Letters* 343, 5 (2001), 633 – 641.
- [63] THEIS, L. S., MOTZOI, F., AND WILHELM, F. K. Simultaneous gates in frequency-crowded multilevel systems using fast, robust, analytic control shapes. *Phys. Rev. A* 93 (2016), 012324.
- [64] WARREN, W. S. Effects of arbitrary laser or NMR pulse shapes on population inversion and coherence. *J. Chem. Phys* 81 (1984), 5437–5448.
- [65] YANG, Z.-C., RAHMANI, A., SHABANI, A., NEVEN, H., AND CHAMON, C. Optimizing variational quantum algorithms using pontryagin’s minimum principle. *Phys. Rev. X* 7 (2017), 021027.